Submitted to Acta Metallurgica

UCRL-20304
Preprint c.2

ON SHORT RANGE ORDER AND MICRO-DOMAINS IN THE Ni_4Mo SYSTEM

P. R. Okamoto and G. Thomas

December 1970

AEC Contract No. W-7405-eng-48

TWO-WEEK LOAN COPY

This is a Library Circulating Copy which may be borrowed for two weeks. For a personal retention copy, call Tech. Info. Division, Ext. 5545

LAWRENCE RADIATION LABORATORY
UNIVERSITY of CALIFORNIA BERKELEY

UCRL-20304 c.2

DISCLAIMER

This document was prepared as an account of work sponsored by the United States Government. While this document is believed to contain correct information, neither the United States Government nor any agency thereof, nor the Regents of the University of California, nor any of their employees, makes any warranty, express or implied, or assumes any legal responsibility for the accuracy, completeness, or usefulness of any information, apparatus, product, or process disclosed, or represents that its use would not infringe privately owned rights. Reference herein to any specific commercial product, process, or service by its trade name, trademark, manufacturer, or otherwise, does not necessarily constitute or imply its endorsement, recommendation, or favoring by the United States Government or any agency thereof, or the Regents of the University of California. The views and opinions of authors expressed herein do not necessarily state or reflect those of the United States Government or any agency thereof or the Regents of the University of California.

ON SHORT RANGE ORDER AND MICRO-DOMAINS IN THE Ni_4Mo SYSTEM

P. R. Okamoto and G. Thomas

Inorganic Materials Research Division, Lawrence Radiation Laboratory, Department of Materials Science and Engineering, College of Engineering, University of California, Berkeley, California

ABSTRACT

Electron diffraction and field ion microscopy have been used to investigate the nature of short range order in as quenched Ni_4Mo. The results indicate that the as quenched state consists of an assembly of microdomains possessing the six orientational variants of the Ni_4Mo superstructure. The $1\frac{1}{2}0$ diffuse peaks have been attributed to the occurrence of non-conservative anti-phase boundaries within the micro-domains during which the APB's transform from the non-conservative to the conservative type. A similar argument is used to account for the occurrence of $1\frac{1}{2}0$ peaks in the disordered α-phase at other compositions in the Ni-Mo system.

I. INTRODUCTION

Many stoichiometric solid solution exhibit long range order (LRO) below a critical temperature and short range order (SRO) above it. Perfect LRO is an abstraction valid only at absolute zero and perfect stoichiometry. Any deviation from these ideal conditions necessarily implies a deviation from perfect order which may be characterized in terms of crystalline defects such as a periodic distribution of anti-phase boundaries (APB's) in the case of the long period superlattices. The statistical disorder present in the SRO state above the critical temperature has also frequently been characterized in terms of structural imperfections. The splitting of the diffuse peaks in Cu_3Au[1-3] and $CuAu_3$[4], for example, have been attributed to the occurrence of a more or less regular arrangement of APB's within the tiny ordered regions or micro-domains thought to be present in the disordered state.

In this respect, the recent computer simulation experiments of Gehlen and Cohen[5] are of some interest. They have demonstrated that a specified degree of SRO can indeed be associated with a characteristic microdomain structure. The computer technique leads not only to a clearer interpretation of the statistical information about the near neighbor configuration around an atom but also to three dimensional "pictures" of the microdomain structure. The boundaries between micro-domains are clearly recognizable as APB's or twin boundaries. Moreover, Cohen[6] has noted that the split diffuse peaks in disordered Cu_3Au[3] suggest a domain size of about 12Å in agreement with his computer models.

Nevertheless, the fact that the computer approach or for that matter structural approaches in general are not directly related to the energetics of the system raises some question as to whether such

models have any real physical significance. Statistical-thermodynamic treatments of ordering for example can account for the diffuse scattering distribution without recourse to any particular structural features and therefore implies that they may not be essential for a description of the equilibrium disordered state. Clapp and Moss[7,8] for instance have shown that the intensity of the diffuse peaks is determined by the Fourier transform $V(\bar{k})$ of the interaction potential $V(R)$. Their theory predicts that the diffuse peaks should occur at points in reciprocal space where $V(\bar{k})$ is a minimum. Moreover Moss[9] has recently shown that the splitting of the diffuse peaks in Cu_3Au and $CuAu_3$, previously attributed to APB's within the microdomains, can now be directly related to the shape of the Fermi surface, in particular to the flat regions of the surface where a local minimum in the $V(\bar{k})$ function occurs.

Although the validity of structural models have been seriously questioned, Cowley[10] has recently justified the microdomain concept of SRO from physical arguments. He points out that a local minimum in $V(\bar{k})$ will lead to a long range oscillatory interaction potential which at high temperatures could lead to a lowering of the free energy of the system by the occurrence of nearly periodic arrangement of APB's within the microdomains. On the assumption that a microdomain structure should lead to a minimum electron free energy contribution he suggests two conditions that should be satisfied in order that a microdomain model be valid: (1) the microdomains can be described in terms of a chemically reasonable ordered structure and (2) the structure must produce superlattice reflections which coincide with the positions of the diffuse

peaks corresponding to the minima of the $V(\bar{k})$ function.

These conditions would appear to rule out a microdomain structure for ordering systems in which the diffuse peaks do not coincide with the superlattice reflections of some known ordered phase in the system.

An example would be the controversial Ni-Mo system shown in fig. 1. The structure of the disordered primary and solid solution is fcc. Diffraction patterns of the α-phase exhibit diffuse peaks at all equivalent $1\frac{1}{2}0$ positions in the fcc reciprocal lattice over a wide range of compositions (8-33 at% Mo).[11-13] Within this composition range several ordered structures have been observed. In addition to the β-phase (Ni_4Mo)[12] and γ-phase (Ni_3Mo)[13] a mestable phase (Ni_2Mo)[14] possessing a Pt_2Mo superlattice has been observed in the two phase (β + γ) region. None of these ordered phases produces superlattice reflections at the $1\frac{1}{2}0$ positions. Other systems for which similar phenomena occur are the Ni-W[15] and Au-Cr[16]. In view of this some investigators have rejected the microdomain concept of SRO for these systems.[8,16]

However, Ruedl et al.[17] have obtained dark field electron micrographs of as quenched Ni_4Mo exhibiting a high density of tiny bright dots which they interpreted as direct evidence of a microdomain structure. Moreover, LeFevre et al.[18] have observed a microdomain structure in field ion micrographs in as quenched Ni_4Mo aged for very short times. Therefore, the nature of SRO in the Ni-Mo system is still a matter of considerable controversy.

In view of these controversies and because the Ni-Mo system potentially offers the solution concerning the generality of the microdomain concept of SRO, a detailed investigation by electron diffraction

and field ion microscopy has been carried out to study the very early stages of ordering in Ni_4Mo. The primary object of the study was to correlate changes in the diffuse scattering distribution with the corresponding microstructural changes on the field ion level.

The results taken as a whole confirm the concepts of a microdomain structure and suggest that the $1\frac{1}{2}0$ peaks are associated with imperfectly ordered regions with the DO_{22} superstructure resulting from the occurrence of non-conservative APB's within microdomains. A mechanism is discussed whereby other ordered structures in the Ni-Mo system can be generated from one another by such planar defects. This idea predicts that the $1\frac{1}{2}0$ peaks should be observed in the disordered state of all these ordered phases in agreement with observation.

2. CRYSTALLOGRAPHY OF Ni_4Mo*

The lattice parameter of the disordered fcc phase of the composition Ni 20 at.% Mo is $A_{fcc} = 3.6086\mathring{A}$. Upon ordering, a slight contraction occurs along one of the original cube axes so that the parent fcc lattice becomes face centered tetragonal with $(c/a)_{fct} = 0.986$. The Bravais lattice changes from face centered cubic to body centered tetragonal with $(c/a)_{bct} = 0.623$.[12]

An (001) plan view of the ordered Ni_4Mo is shown schematically in fig. 2a,b for the case where the c-axis coincides with the [001] cube axis. For a given choice of c-axis the Ni and Mo atoms can be arranged in two ways resulting in a bct unit cell containing 8 Ni and 2 Mo atoms

---

* Except where noted all planar and directional indices will be referred to the fcc lattice of the disordered state.

rotated in either a counter-clockwise (fig. 2a) or clockwise sense as in fig. 2b. The two ordering schemes will be referred to as type I and type II structures, respectively.

The type I structure can be generated by a regular layering sequence of Ni and Mo atoms on the $(4\bar{2}0)$ or (240) planes in which every fifth plane contains only Mo atoms, the intervening four only Ni atoms. Therefore a two-fold degeneracy exists with regard to stacking in the sense that the pair of mutually orthogonal planes are crystallographically equivalent with respect to this particular mode of layering; layering on one set of planes leads to an identical layering mode on the other. The same layering mode on the (420) or $(2\bar{4}0)$ planes will generate the type II structure shown in fig. 2b. Similar layering on the remaining mutually orthogonal pairs of planes of the type $\{4\bar{2}0\}$ will generate type I or II structures with the c-axis along either the [010] or [100] cube axes.

It is readily apparent that because of the two-fold degeneracy, if such layering were to occur normal to each of the 12 $\{4\bar{2}0\}$ planes in different parts of a single crystal, the resulting structure will then be an assembly of domains or transformation twins having one of six possible orientational variants relative to the parent fcc lattice. The symmetry planes relating the twins are of the {110} family.

The superposition of the reciprocal lattices of 6 twins results in superlattice reflections arranged symmetrically in groups of four about all equivalent $1\frac{1}{2}0$ positions in the fcc reciprocal lattice. The (002), (121) and sections of the fcc reciprocal lattice are shown schematically in fig. 3a and b.

The structure factor for the fundamental and superlattice reflections are given by:

$$F_f^{D1a} = 2(f_{Mo} + 4f_{Ni}) \qquad \text{(for } H-K+L = 2n(n = 0, 1, \ldots)$$

$$F_S^{D1a} = 2S(f_{Mo} - f_{Ni}) \qquad \text{(for } H+K+L = 2n(n = 0, 1, \ldots)$$

$$\text{(and } 2H+K \neq 5n)$$

where S is the Bragg-Williams LRO parameter and H, K, and L refer to the bct unit cell. If h, k and l refer to the fcc unit cell, then for the type I structure with the c-axis along 001_{fcc} (fig. 2a),

$h = (3H-K)/5$, $k = (H+3K)\ 5$ and $l = L$.

3. EXPERIMENTAL PROCEDURE

Alloys of nominal composition Ni 29.1 wt% Mo (20 at.% Mo) were prepared from 99.9% Ni and 99.9% Mo by arc melting in argon. In order to obtain a dense, gas-free alloy, the ingot was swaged into rod form then remelted four times in an electron beam zone refining furnace. The rod was inverted between each pass to ensure uniform mixing of the constituents. The final homogenization treatment consisted of holding in vacuum for an additional 90 hours at 1250°C. The composition of the homogenized rod was determined by wet chemical analysis to be Ni 29.3 wt% Mo (20.2 at.% Mo). Sheets .005 in. thick were produced by cold-rolling the rods at room temperature using intermediate anneals at 1100°C.

Samples with dimensions 0.25 x 0.005 x 1.0 in. were sealed in evacuated quartz tubes and placed in a vertical tube furnace for 3 hours at 1100°C. Quenching was performed by releasing the quartz tube into iced brine.

Isothermal aging treatments were performed in a salt bath solution

of $BaCl_2$, NaCl and $CaCl_2$. Heating rates were measured using .005 in. dia. Pt-10% Rh thermocouples spot welded to the sample with the output connected either to an oscilloscope or a honeywell Electronik 19 strip recorder. The minimum aging time used for any heat treatment was arbitrarily chosen to be twice the time required for the sample temperature to reach equilibrium. For example, for 650°C and 750°C the average time to reach equilibrium was 2 and 5 seconds, respectively. Hence, for these aging treatments the shortest aging times involved were 4 and 10 seconds, respectively. For aging times less than one minute, the maximum temperature fluctuation of the sample was $\pm$ 5°C. For longer times, the fluctuations were generally maintained below $\pm$ 2°C. The quenching rates during the transfer from the salt bath to an iced brine solution was also monitored and the time to reach zero output on the strip recorder was kept consistently below one second.

Specimens for both TEM and FIM were prepared from the same heat treated sample. FIM specimens were prepared by cutting 10 to 15 strips 1 inch long and approximately .005 inches wide from each sample using a specially designed precision shearing device. In order to check whether spurious effects were introduced by the shearing process, several strips were precut from an as-quenched sample. These together with another as-quenched sample were sealed in evacuated quartz tubes and aged for 125 hours at 750°C to develop the fully ordered state. FIM images from the precut strips and those cut from the sample after aging were very similar, neither revealing any evidence of disorder. Any deformation which may have occurred during the shearing process was, therefore, confined to the surface and subsequently removed during

electropolishing.

Thin foils suitable for TEM were prepared by electropolishing with a solution containing 16 ml perchloric acid, 132 ml ethyl glycol, 16 ml hydro fluoric acid and 16 ml distilled water. FIM specimens were prepared by the double layer method in which the tip of the specimen is dipped into a thin layer of electrolyte floating on top of a bath of carbon tetrachloride.

4. EXPERIMENTAL RESULTS

4.1 Electron Diffraction

4.1.1 As-quenched Alloys

Figure 4a is an [001] selected area diffraction pattern obtained from an alloy which had been quenched from 1100°C into iced brine. In agreement with the x-ray results of Spruiell and Stansbury,[12] intensity maxima are observed at all equivalent $1\frac{1}{2}0$ positions of the fcc reciprocal lattice. The asymmetry in the intensity distribution of the 200 fundamental reflections is also in agreement with their x-ray work. They attribute the higher intensity on the low angle side to a size effect, in this case indicating that Mo atoms have a larger diameter in solution than Ni atoms. Figure 4a is also similar to the [001] electron diffraction patterns of Au_3Cr reported by Tanner. However, their patterns were obtained at temperature 500°C above the critical ordering temperature for Au_3Cr, so that the $1\frac{1}{2}0$ maxima were quite broad compared to those in fig. 3a.

Figure 4b is a [121] diffraction pattern of the same specimen. Again weak maxima are observed at $1\frac{1}{2}0$ positions. However, this pattern also exhibits features which have not been reported in earlier

studies, namely, the presence of diffuse streaks passing through $1\frac{1}{2}0$ peaks with weak intensity maxima near, but not exactly at, the equilibrium angular positions corresponding to superlattice reflections of the fully ordered Ni_4Mo. These intensity maxima are not directly observable on the fluorescent screen in the microscope viewing chamber and were first discovered on microphotometer tracings. In fact, they are generally not discernible even on the original photographic plates unless precautions are used to avoid overexposing the diffraction patterns. The best results are obtained by fully defocussing the second condensor lens and then exposing for long times (1-2 minutes).

Figure 4b is a reproduction of the best of many original photographic plates obtained during this study. The microphotometer tracing obtained from the original plate is shown in fig. 5. The weak intensity maxima near the $2\bar{2}0$ and $3\bar{3}0$ bct superlattice positions are clearly detectable while those near the $1\bar{1}0$ and $4\bar{4}0$ positions are all but obscured by the neighboring $1\frac{1}{2}0$ intensity peak. These weak intensity maxima were not observed on the [001] diffraction patterns. This is not surprising, however, since in this particular orientation they would all lie very close to and hence be obscured by one of the $1\frac{1}{2}0$ maxima. As indicated in fig. 5, the weak maxima are detectable only when their neighboring $1\frac{1}{2}0$ maxima do not lie on the reflecting sphere. This will occur only for certain favorable orientations and the most favorable of all would be one where <u>only</u> superlattice reflections lie on the reflecting sphere. The $[\bar{1}30]$ orientation is one of these and as shown in fig. 4c exhibits quite clearly weak intensity maxima near all superlattice positions.

To our knowledge, the existence of weak intensity maxima near the superlattice positions in as-quenched Ni_4Mo has not been previously reported. This is obviously due in part to the weakness of these particular maxima but more likely due to the fact that past diffuse scattering studies for this alloy have been confined almost exclusively to the (002) reciprocal lattice section. As just pointed out, this particular orientation is the least convenient one of all for such purposes. The existence of weak intensity maxima near the superlattice positions in the as-quenched alloy is quite significant since their apparent absence in past studies have been one of the reasons for arguing against the existence of microdomains in disordered Ni_4Mo. The present observations, however, suggest some form of microdomain structure similar to the one described in Section 2 must exist in as-quenched Ni_4Mo.

4.1.2 Alloys Aged at 650°C

Upon aging at 650°C rather unusual and interesting changes occur in the diffraction patterns during the first ten minutes. These changes are shown in fig. 6a-d.

After 5 minutes of aging the weak intensity maxima near the superlattice reflections are clearly detectable without the aid of a microphotometer. They appear on [001] diffraction patterns (fig. 6b) as diffuse satellites about the $1\frac{1}{2}0$ positions broadened in directions parallel to $\langle 2\bar{1}0\rangle$ directions. In [121] patterns (fig. 6a) the satellites near a $1\frac{1}{2}0$ SRO maxima are broader and more intense than those away from such position. The effect is even more pronounced after 10 minutes of aging (fig. 6c). This asymmetry is not observed in [001] diffraction

patterns.

Tilting experiments show that the satellites about a $1\frac{1}{2}0$ SRO maxima have a paddle-like shape shown schematically in fig. 7a. Each broad flat face is normal to a [001] direction and these are the sections observed in [001] diffraction patterns. From an examination of the composite reciprocal lattice it is apparent that in a $[121]_{fcc}$ orientation, the reflecting sphere will cut through the satellite at the sections A and B.

Section A corresponds to satellites near $1\bar{1}0$ and 440 bct superlattice positions, i.e., to those which appear to emanate from a $1\frac{1}{2}0$ SRO spot. Section B corresponds to satellites near $2\bar{2}0$ and $3\bar{3}0$ bct positions whose neighboring $1\frac{1}{2}0$ spot lie off the reflecting sphere.

The marked broadening of the satellites in the <210> directions suggests that the ordered domains may exist as thin layers lying parallel to the $\{420\}_{fcc}$ planes. This would be compatible with the layered structure of the fully ordered Ni_4Mo structure discussed in Section 2. This type of plate-like morphology has in fact been reported in Co-Pt[19] and Cu-Au[20] alloys at the 50-50 composition. In these alloys superlattice planes are also layered such that alternating planes contain atoms of one type only. The most prominent superlattice plane is the (002) which is also the reported habit plane for the plate-shaped domains.

However, the diffraction patterns of Ni_4Mo exhibit certain distinctive features during this stage of ordering which are not compatible with a simple plate-like morphology. The patterns show a definite asymmetry in that reflections which would normally arise from domains of a particular orientational variant are not broadened in the same <210>

directions. This effect, shown schematically in fig. 7b, is most pronounced in [001] diffraction patterns, (see Section 5).

4.1.3 Alloys Aged at 750°C

The ordering reaction at 750°C is extremely fast. Alloys aged at this temperature reach a fairly advanced stage of order by at least 5 seconds, the shortest aging time used for this series of experiments. As shown in fig. 9a, well defined superlattice reflections are observed though slightly broadened in <210> directions. Although $1\frac{1}{2}0$ intensity peaks are still observed their intensity is relatively weak compared to alloys aged 10 min. at 650°C.

A marked rounding out of the superlattice reflections occurs by 10 seconds of aging (fig. 10a) and is accompanied by the disappearance of the $1\frac{1}{2}0$ peaks. However, the diffraction patterns now exhibit weak double diffraction spots. Ruedl[11] has shown that at more advanced stages of ordering where the domains are sufficiently large, the double diffraction spots can be used quite effectively to image the twin boundaries themselves.

4.2 Microstructure

Although repeated attempts were made, it was impossible to resolve microdomains in dark field electron micrographs of as-quenched specimens using either a $1\frac{1}{2}0$ spot or one of the diffuse superlattice reflections.

In alloys aged at 650°C a distinct microdomain structure was observed only after 10 minutes of aging. Figure 8d is a $1\frac{1}{2}0$ dark field image which appears very similar to the tiny bright dots reported by Ruedl et al.[15] in their as-quenched alloys. The domains appear equiaxed and are about 20Å in diameter. The image remains essentially

unchanged if one uses one of the broad superlattice reflections; this is not entirely surprising since at this stage of ordering the two types of reflections overlap. Figure 8b is a $1\frac{1}{2}0$ dark field micrograph of an alloy aged 5 minutes at 650°C. Although some form of mottling is apparent in the thinner regions the distinct bright dotted contrast of fig. 8d is absent. In both samples, however, dark field images using fundamental reflections exhibit a striated or tweed type contrast characteristic of alloys containing a large volume fraction of coherent precipitates.[21]

Figures 9b and 10b are dark field micrographs of alloys aged at 750°C for 5 and 10 seconds respectively. Both images were formed using a superlattice reflection. The domains are equiaxed and have very similar size distribution ranging from about 20 to 100Å. A slight tendency for the domains of a particular variant to align themselves in rows was observed with longer aging times but neither with sufficient frequency nor with sufficient directional uniqueness to establish any definite relationship with a diffraction effect.

It appears, therefore, that the marked weakening of the $1\frac{1}{2}0$ spots along with the rounding out of the superlattice reflection are not connected with the average domain size since it remains essentially unchanged. It is also apparent that the broadening of the superlattice reflection in the <210> directions cannot be wholly a shape factor effect as the domains appear equiaxed from the very earliest stages of ordering.

Figures 9c-f are bright field images using various fundamental reflections from an [110] foil. In each case the foil was tilted so that only one strong beam was operating. The striated contrast is

observed to change with operating reflection in a manner similar to that observed in Cu-Be alloys[21] and other systems (see e.g. ref. 22 for review) during the very early stages of coherent phase transformation.

4.3 Field Ion Microscopy

The most significant diffraction effects of this investigation were found to occur during the first 10 minutes of aging at 650°C. Although transmission electron microscopy failed to reveal a microdomain structure in the as-quenched alloy and in alloys aged only 5 minutes, evidence for their existence was obtained by field ion microscopy.

Figures 11a, b depict the microsturctures of the as-quenched alloy. The images are highly irregular exhibiting the fcc symmetry of the disordered state. The stability was found to depend markedly on the specimen temperature. When liquid helium was used as specimen coolant (fig. 11a) the image was very stable which allowed controlled field evaporation techniques to be used to examine the specimen layer by layer. The only features of note were the planar defects indicated by arrows in fig. 11a. These defects persist only for two or three layers before disappearing. These defects are not twin or grain boundaries as all the poles are in the correct angular positions. When liquid nitrogen is used as specimen coolant image stability is lost. The sample slowly field evaporates in an irregular fashion. However, certain clusters of atoms were found to be relatively stable in that surrounding regions field evaporate at slightly lower fields. These clusters, therefore, protrude locally and so act as more effective emission centers (fig. 11b). The distribution of these clusters is not random. They tend to appear most frequently around the <420> poles marked by circles

in fig. 11b. Moreover they were found to persist in aged alloys. Figure 12a and b are examples obtained from samples aged 5 and 10 minutes. Both micrographs were part of field evaporation sequences. In fig. 12a the <420> poles are marked by circles. Those in which bright atom clusters are observed are marked by arrows. By use of pulse field evaporation techniques it was found that the smaller clusters field evaporate as a group. In some instances the clusters are large enough to be recognized as partial rings. In any case, however, these relatively stable groups of atoms never persist for more than one or two layers. Although some groups are occasionally observed near <620> poles they appear most frequently about the <420> poles.

After 10 minutes of aging all the clusters are sufficiently large to be recognized as portions of small partial rings. The discontinuity between adjacent rings shows that they are tiny domains of different orientational variants. As shown in fig. 12b these partial rings indicated by arrows are located at or very near <420> poles.

4.4 Summary of Experimental Results

The significant features of this investigation to be discussed in the next section are:

(1) Diffuse superlattice reflections of the ordered Ni_4Mo structure are observed in as-quenched alloys in addition to $1\frac{1}{2}0$ SRO peaks, but only in certain favorable orientations.

(2) The superlattice reflections are broadened in the <210> directions but reflections corresponding to a particular orientational variant are broadened in different but mutually orthogonal <210> directions.

(3) At 750°C the decrease in broadening is accompanied by a decrease in the intensity of the $1\frac{1}{2}0$ peaks but is not accompanied by a change in the shape nor size distribution of the domain.

5. DISCUSSION OF RESULTS

The most significant result of this study is the observation of diffuse superlattice reflections in the as-quenched alloy. Their existence proves that microdomains possessing all six possible variants of the ordered Ni_4Mo structure exist in the as-quenched state.

This conclusion is supported by the fact that FIM images exhibit unusually bright and stable groups of atoms whose distribution and frequency of appearance have a strong orientational dependence on the <420> poles. The fact that these poles are normal to the layered planes with largest d-spacing means that they are superlattice planes on which the Mo atoms are most densely packed. Moreover the fact that Mo atoms are preferentially imaged in Ni_4Mo suggests that the bright atom clusters are the pure Mo or Mo-rich planes.

It is obvious that if microdomains possessing all six possible variants are distributed throughout the FIM tip a domain intersecting the specimen surface at a particular <420> pole will have one chance in six of having its layered planes normal to this pole. Therefore, by focussing attention on the <420> poles in the FIM image we should while field evaporating periodically observe bright atom clusters corresponding to Mo planes of suitably oriented domains.

5.1 Antiphase Domains

The broadening of the superlattice reflections in the <210> directions is not wholly a shape factor effect as the domains are equiaxed even in

alloys aged 10 min. at 650°C where broadening was most pronounced.

A more likely source of broadening would be the occurrence of antiphase boundaries (APB) within microdomains of all the six orientational variants. If the boundaries were spaced in a periodic manner the superlattice reflection would split into satellites but if the boundary spacing is irregular the satellites would wash out and the superlattice would simply be broadened in a direction normal to the plane of the APB.[23,3] The fact that the superlattice reflections are broadened in the <210> directions implies the APB's lie parallel to the {420} planes. Since the possible antiphase vectors are lattice vectors of the disordered fcc structure they will be of the form P = 1/2<110>. Consequently the APB must necessarily be of the non-conservative type. Examples of both conservative and non-conservative APB's are illustrated in fig. 13.

In fig. 13a the APB specified by $(110)1/2[1\bar{1}0]$ was formed by translating the crystal on the right side of the (110) boundary by the vector $P = 1/2[1\bar{1}0]$. As this vector lies in the plane of the APB, no atoms were removed and no local changes in composition occur across the boundary. Such APB's are called conservative. A pair of non-conservative APB's of the form $(420)1/2[1\bar{1}0]$ and $(420)1/2[\bar{1}10]$ are illustrated in fig. 13b and 13c, respectively. In fig. 13b a plane containing all Ni atoms was removed in order to form the boundary while in fig. 13c an extra plane of Ni atoms was added. In both cases the local composition across each boundary has been altered from the average value, but not across the pair. In general, the number of planes removed or added is given by the product $\vec{g}.\vec{p}$ where $\vec{g}$ is the reciprocal

lattice vector normal to the APB and $\vec{p}$ is the shift vector. For the APB's illustrated in fig. 13a, b and c, $\vec{g}.\vec{p}$ = 0, 1, -1, respectively where the sense of $\vec{g}$ was chosen so that a minus sign corresponds to an addition of a plane. For APB's of the type {420}1/2<1$\bar{1}$0> the product $\vec{g}.\vec{p}$ takes on the values $\pm$ 1, $\pm$2 and $\pm$3 only.

Due to the change in local composition across non-conservative APB's their energy will be higher relative to conservative APB's.[24,25] However, non-conservative APB's may occur to accommodate local fluctuations in composition. Moreover, such APB's are likely to occur as closely spaced pairs so that the local composition across the pair is not changed. Such pairing may not occur at all, however, since the APB energy is proportional to the degree of order present. Therefore, the difference in energy between conservative and non-conservative APB's will be very small in partially ordered alloys and may effectively vanish in as-quenched alloys and those aged for very short times. However, as the degree of order increases with aging time the non-conservative APB's will tend to form conservative APB's if diffusion can occur. This process should result in a decrease in the broadening in the superlattice reflections in the <210> directions.

That the above process may actually occur is supported by the changes in the shape of the superlattice reflections on aging at 750°C. Comparison of figs. 9a and 10a shows a marked rounding out of the superlattice reflections with aging time. As was mentioned in Section 4, the rounding out process was not accompanied by any noticeable change in shape nor in the size distributions of the microdomains. Therefore, the essential change must have been increase in the degree of order within

the microdomains.

A comparison of fig. 9a and 10a also shows that the rounding out process is accompanied by a decrease in the intensity of the $1\ \frac{1}{2}\ 0$ SRO peaks. The implication is that the presence of $1\ \frac{1}{2}\ 0$ peaks and non-conservative APB's are directly related.

That this is likely to be the case can be seen by referring again to fig. 13b. This schematic shows that the local compositional change across the APB occurs in the form of a change in the stacking sequence normal to the (420) planes from BAAAAB to BAAAB. In other words, immediately to the left of the APB the stacking sequence is such that every fourth (420) plane is a pure Mo plane. As illustrated in fig. 14 this stacking sequence generates the DO_{22} structure which will produce superlattice reflections at certain $1\ \frac{1}{2}\ 0$ and 100 positions in the fcc reciprocal lattice.[16] Hence, a non-conservative APB such as fig. 13b can always be associated with a thin layer of DO_{22} material at least one unit cell thick. When this transforms to a conservative APB the DO_{22} layer is removed and the broadening of the superlattice reflections in the <210> directions should vanish along with the $1\ \frac{1}{2}\ 0$ spots.

It is apparent from fig. 2 and 14 that both the Dl_a (Ni_4Mo) and DO_{22} superstructures can be generated by stacking of Mo and Ni planes in proper sequences. If λ is the number of (420) atomic planes between pure Mo planes then for Ni_4Mo $\lambda = 5$ and for DO_{22} $\lambda = 4$. If such stacking were to occur in all 12<210> directions in different parts of a crystal, one will obtain six orientational variants for $\lambda = 5$ but only 3 distinct variants for $\lambda = 4$. This is because the Dl_a structure has a two-fold degeneracy with regard to a BAAAAB stacking sequence on the {420} planes

while the DO_{22} with its BAAAB form has a four-fold degeneracy. For example a BAAAB stacking on the (420) plane leads to identical stacking on the $(4\bar{2}0)$, (204) and $(20\bar{4})$ planes.

This means that if non-conservative APB's of the form $\{420\}1/2\langle 1\bar{1}0\rangle$ occur within microdomains of all the 6 variants of Ni_4Mo a significant volume fraction of the entire system would in effect possess the DO_{22} structure having one of the three possible variants. Consequently, the diffraction pattern should also exhibit DO_{22} superlattice reflections which occur not only at all equivalent $\{1\ \frac{1}{2}\ 0\}$ positions but also at all equivalent {100} positions in the fcc reciprocal lattice.

However, superlattice reflections are not observed at the {100} positions. But the arguments which lead us to expect their presence was based on fig. 13 which applies to perfectly ordered Ni_4Mo. As pointed out earlier non-conservative APB's are expected to exist only when the degree of order is very small. In the next section we will determine the conditions for which the {100} superlattice reflections can vanish.

5.2 Long Range Order Diffraction Effects

The state of LRO in an alloy can be described in terms of a system of interpenetrating sublattices and a complete set of occupational parameters specifying the distribution of the atomic species on each sublattice. For layered structures such as the $D1_a(Ni_4Mo)$ and DO_{22} the (420) planes contain sublattice sites of one type only. The number of kinds of sublattice sites is equal to λ the number of (420) planes between pure Mo planes, i.e. $\lambda = 5$ for the $D1_a(Ni_4Mo)$ and $\lambda = 4$ for the DO_{22} structure. Hence, if the form composition fluctuation is known in the direction normal to

the (420) planes the occupational parameters of each sublattice are also known. This is shown schematically in fig. 15 for $\lambda = 5$, i.e. the $Dl_a(Ni_4Mo)$ structure. In order to obtain the perfectly ordered structure the composition fluctuation must have the form shown in fig. 15b. For a partially ordered alloy it must have the form shown in fig. 15c if the degree of order is to be specified by a single LRO parameter. If the form of the composition fluctuation is sinusoidal as shown in fig. 15d, two LRO parameters are required to specify the degree of order. The number of independent LRO parameters is equal to the number of different kinds of superlattice reflections which are expected to appear in diffraction patterns.

The fully ordered (fig. 15b) and the partially ordered states (fig. 15c) require only a single LRO parameter so that all superlattice reflections have the same structure factor and hence the same intensity. Figs. 6a and b indicate that the intensity of diffuse superlattice reflections are not the same but that those near a $1\frac{1}{2}0$ spot are much more intense than those away from $1\frac{1}{2}0$ spots. This suggests that the composition fluctuation within microdomains at this stage of ordering is of a form closer to that illustrated in fig. 15d than in 15c. However, it cannot be perfectly sinusoidal as otherwise the weaker reflections should disappear entirely. In order to see physically why this should occur, one can simply recall how the so-called "side" bands form in a two dimensional crystal whose planar atomic scattering factor varies sinusoidally. A side band will form symmetrically about each matrix reflection at a distance inversely proportional to the fundamental wavelength λ in the direction of the fluctuation.

If the modulation is of the form of a repeating delta function as in fig. 15b, all higher harmonics ($n = 1, 2, \ldots \lambda$) must be present; the nth producing a side band at a distance $\pm (n\lambda)^{-1}$ from a matrix reflection. The intensity of each side band will be proportional to the amplitude of the corresponding harmonic. If the amplitude is small the intensity of the corresponding side band (or superlattice reflection) will be weak.

There is additional evidence that composition modulation exists within the microdomains. It was pointed out in Section 4.1.2 that the broadening of D1a the superlattice reflections exhibit an asymmetry in that of the superlattice reflections corresponding to a particular orientational variant half are broadened in one <210> direction while the other half in a <210> direction normal to the first.

If the composition modulation were of the form illustrated in fig. 15c then each variant, as described earlier, would have a two-fold degeneracy with regard to stacking on two mutually orthogonal planes of the form {420}. Consequently non-conservative APB's of the form $\{420\}1/2\langle 1\bar{1}0\rangle$ would tend to form on each with equal probability. Therefore, broadening effects should occur in two perpendicular directions and superlattice reflections should appear circular in an [001] diffraction pattern.

However, this two-fold degeneracy is removed if the composition modulation is of the form shown in fig. 15d. For example, if the composition varies sinusoidally in the [210] direction, the form of the variation in the $[1\bar{2}0]$ will not have a simple sinusoidal wave form. Since each <210> direction is unique with respect to a simple sinusoidal variation there are in effect 12 orientational-compositional variants and the asymmetry of the superlattice reflections can be explained if

the non-conservative APB's form preferentially on the {420} planes normal to direction of the sinusoidal variation.

On the other hand, the four-fold degeneracy associated with the DO_{22} superstructure is independent of the form of the compositional variation so long as the periodicity is four (420) atomic spacings. Although the thin DO_{22} regions associated with non-conservative APB's might cause shape factor broadening, the $1\ \frac{1}{2}\ 0$ superlattice reflections of a particular variant would be broadened in four <210> directions so should appear more or less spherical in shape in agreement with observations.

In order to determine the disappearance conditions for the {100} superlattice reflections, we have calculated the three dimensional structure factor for the DO_{22} structure in terms of the occupational parameters x_{BI}, x_{BII}, x_{BIII}, and x_{BIV} specifying the composition of the sublattices in at.% B. The relative positions of the sublattice sites are shown in fig. 14. Assuming all three variants contribute to the diffraction pattern the results can be summarized as follows:

(1) For matrix reflections:

$$F_f^{DO_{22}} = 8(m_A f_A + m_B f_B)$$

(2) For all equivalent $\{1\ \frac{1}{2}\ 0\}$ superlattice reflections:

$$F^{DO_{22}}_{\{1\ \frac{1}{2}\ 0\}} = 2[(x_{BI} - x_{BII})^2 + (x_{BIII} - x_{BIV})^2]^{1/2}(f_B - f_A)$$

(3) For all equivalent {100} superlattice reflections:

$$F^{DO_{22}}_{\{100\}} = 2[(x_{BI} + x_{BII}) - (x_{BIII} + x_{BIV})](f_B - f_A)$$

(4) For perfect DO_{22} ordering:

$$x_{BI} = 1,\ x_{BII} = x_{BIII} = x_{BIV},\ m_B = \frac{1}{4}$$

$$\therefore F^{DO_{22}}_{\{1\ \frac{1}{2}\ 0\}} = F^{DO_{22}}_{\{100\}}$$

For complete disorder:

$$x_{BI} = x_{BII} = x_{BIII} = x_{BIV} = m_B$$

$$\therefore F^{DO_{22}}_{\{1\ \frac{1}{2}\ 0\}} = F^{DO_{22}}_{\{100\}} = 0$$

(5) For sinusoidal compositional waves of the form $x_{BP} = A(1 + \cos \frac{2\pi P}{\lambda})$

with $\lambda = 4$ atomic spacings and $P = 0, 1, 2, 3$.

$1/2x_{BI} = x_{BIII} = x_{BIV}$ and $x_{BII} = 0$

$$F^{DO_{22}}_{\{1\ \frac{1}{2}\ 0\}} = 2x_{BI}(f_B - f_A)$$

$$F^{DO_{22}}_{\{100\}} = 0$$

The composition range for which the condition (5) is satisfied can be determined by requiring that the number of B atoms on all the sublattices be equal to the total number of lattice sites time the average composition m_B, i.e.,

(6) $x_{BI} + x_{BII} + x_{BIII} + x_{BIV} = 4m_B$

When (5) is satisfied (6) reduces to $x_{BI} = 2m_B$. Since x_{BI} must always lie between zero and unity m_B must lie between 0 and 1/2. Hence, this includes the observed range (8 - 33 at.% Mo) over which $1\ \frac{1}{2}\ 0$ spots are observed in

the α phase.[11-14] The intensity of the $1\frac{1}{2}0$ spots will be proportional to m_B^2 and hence should decrease rapidly with increasing Ni content.

It is significant that the first ordered phase to form in the β + γ region after quenching from the α phase is the metastable Ni_2Mo.[14] The structure of the ordered phase is shown in fig. 16. It can also be generated by stacking of pure Mo and Ni planes, with λ = 3. Six distinct orientations can be formed by stacking on different {420} planes. As in the case for the Dl_a structure a two-fold degeneracy occurs with regard to stacking planes, but in this case the pair of equivalent planes are non-orthogonal pairs, e.g. $(2\bar{4}0 - 4\bar{2}0)$; (240 - 420) etc.

Consequently the same arguments concerning non-conservative APB's of the form $\{420\}1/2\langle 1\bar{1}0\rangle$ can be used to explain the $1\frac{1}{2}0$ SRO peaks in the α-phase in the β + γ composition range providing the α phase consists of a microdomain possessing the 6 possible orientational variants of the Ni_2Mo superstructure.

It is obvious that the three ordered structures $Dl_a(Ni_4Mo)$, DO_{22} and Ni_2Mo are closely related. Starting with any one of the three superstructures, a transformation to the other two kinds can be accomplished by the introduction a periodic distribution of $\{420\}1/2\langle 1\bar{1}0\rangle$ APB's. For example, a (420)1/2[101] APB in a type II Ni_4Mo structure will produce a layer of the Ni_2Mo structure adjacent to the APB. This has been confirmed during recent low temperature annealing experiments. An extensive account of these observations will be reported in a subsequent paper.[26]

which arise from the presence of periodic APB's at every M_1 ($= \frac{a_1^*}{m_1}$) and M_2 ($\frac{a_2^*}{m_2}$) cells along the respective directions, as described earlier in sec. 3.5. At temperatures above T_c, if there exist microdomains with the Watanabe type structure, but without any fixed periodicities M_1 and M_2, then there will be no strong superlattice reflections, but a broad diffuse scattering near positions corresponding to all possible periodicities that are present as observed in Fig. 15(b). Since the origin of the satellites in Fig. 14(c) is most likely to be due to periodic lattice modulations or composition modulations in the ℓro state, these will be completely washed out in the sro state because there will be hardly any such periodic modulation present. This explains the absence of any scattering near satellite positions above T_c. Thus the diffuse scattering in Au_3Mn can also be accounted for by the presence of microdomains with Watanabe type structure. The presence of the microdomains of such long period Watanabe type structure in the sro state would necessarily imply that long range interatomic interactions are present. The justification for long range interactions being present in the sro state has been given by Cowley[28] in terms of flat regions being present on the Fermi surface.

5. CONCLUSIONS

1. The high temperature electron diffraction patterns of Au_3Cr and Au_4Cr above T_c show a tetrahedral intensity distribution around the $\{1\frac{1}{2}0\}$ positions which gives rise to diffuse scattering at Dla positions. The comparison of the as quenched state with diffraction patterns taken

above T_c show that the sro state is essentially retained on quenching in this alloy.

2. The diffraction patterns of Au_4V in the sro state also exhibit diffuse scattering at $\{1\frac{1}{2}0\}$ and Dla positions.

3. The diffuse scattering in Au_3Mn above T_c gives rise to an intensity distribution centered around $\{1\frac{1}{2}0\}$ in such a way that weak scattering is present near most of the superlattice reflections corresponding to Watanabe type two dimensional long period superstructure.

4. The sro states of Ni_4Mo and Ni_3Mo show diffuse scattering near Dla and Ni_2Mo superlattice positions in addition to those at $\{1\frac{1}{2}0\}$ positions.

5. The presence of weak scattering near various superlattice positions suggests that in the sro state, Au-Cr and Au-V alloys contain predominantly imperfectly ordered DO_{22} and Dla type microdomains. The Ni-Mo alloys contain imperfectly ordered DO_{22}, Dla and Ni_2Mo type microdomains whereas Au-Mn alloys may contain microdomains with a structure close to that of the Watanabe type long period superstructure.

6. The existing statistical thermodynamic model of Clapp and Moss is unable to explain the shape of $\{1\frac{1}{2}0\}$ spots in Au-Cr and Au-V alloys but can explain most features of diffuse scattering in Au-Mn and Ni-Mo alloys.

7. The classical microdomain concept is not always valid and the sro state may contain more than one type of microdomain. A modified microdomain model is proposed in which the sro state is best described as a mixture of imperfectly ordered microdomains with various types of superstructures in different proportions. This description of sro state is very similar to Clapp's description in terms of clusters.

ACKNOWLEDGEMENTS

This work was supported by the U. S. Atomic Energy Commission through the Inorganic Materials Research Division, Lawrence Berkeley Laboratory, University of California, Berkeley, California. The authors are grateful to Dr. L. E. Tanner for supplying the Au-Mn samples and for helpful discussions and to Dr. P. C. Clapp for his valuable comments.

REFERENCES

1. P. C. Clapp and S. C. Moss, Phys. Rev., 171, 754 (1968).
2. S. C. Moss and P. C. Clapp, Phys. Rev., 171, 764 (1968).
3. J. E. Spruiell and E. E. Stansbury, J. Phys. Chem. Solids 26, 811 (1965).
4. H. G. Baer, Z. Metallkde, 57, 318 (1966).
5. L. E. Tanner, P. C. Clapp and R. S. Toth, Mat. Res. Bull., 3, 855 (1968).
6. J. R. Castles, J. M. Cowley and A. E. C. Spargo, Acta Cryst. A27, 376 (1971).
7. P. R. Okamoto, Ph.D. Thesis, University of California, Berkeley UCRL-19175 (1969).
8. P. R. Okamoto and G. Thomas, Acta Met., 19, 825 (1971).
9. P. C. Clapp, Tech. Rep. No. 249, Ledgemont Laboratory, Kennecott Copper Corporation (1970).
10. P. C. Clapp, J. Phys. Chem. Solids, 30, 2589 (1969).
11. G. Thomas in High Temperature, High Resolution Metallography, Gordon and Breach Science Publishers, N.Y., 217 (1967).
12. D. Harker, J. Chem. Phys., 12, 317 (1944).
13. E. Ruedl, P. Delavignette and S. Amelinckx, Phys. Status Solidi 28, 305 (1968).
14. M. Yamamoto, S. Nenno, T. Saburi and Y. Mizutani, Trans. J.I.M., 11, 120 (1970).
15. S. K. Das and G. Thomas (submitted to Phys. Stat. Solidi).
16. S. Saito and P. A. Beck, Trans. AIME, 215, 938 (1959).

17. E. Ruedl and S. Amelinckx, Mat. Res. Bull., 4, 361 (1969).

18. S. K. Das, Ph.D. thesis, U. C. Berkeley, LBL-176 (1971).

19. H. Sato, R. S. Toth, and G. Honjo, J. Phys. Chem. Solids, 28, 137 (1967).

20. E. Stolz and K. Schubert, Z. Metallkde, 53, 433 (1962).

21. D. Watanabe, J. Phys. Soc. Japan, 15, 1030 (1960).

22. D. Watanabe, J. Phys. Soc. Japan, 15, 1251 (1960).

23. D. P. Morris and J. L. Hughes, Acta Cryst., 15, 1062 (1962).

24. P. C. Clapp (private communication).

25. W. Lin, J. E. Spruiell and R. O. Williams, J. Appl. Cryst. 3, 297 (1970).

26. J. M. Penisson, A. Bourret and Ph. Eurin, Acta Met., 19, 1195 (1971).

27. A. M. Ammons and J. E. Spruiell, J. Appl. Phys. 39, 3682 (1968).

28. J. M. Cowley in The Chemistry of Extended Defects in Non-metallic Solids, Eds. L. Eyring and M. Okeeffe, North Holland, London 259 (1970).

FIGURE CAPTIONS

Fig. 1. (a) [001] reciprocal lattice section containing D1a, Ni_2Mo, $\{1\frac{1}{2}0\}$ sro spots, (b) $[\bar{1}30]$ reciprocal lattice section.

Fig. 2. [001] diffraction pattern of Ni_4Mo quenched in iced brine from 1100°C.

Fig. 3. Iso-intensity contour map of the [001] electron diffraction pattern of quenched Ni_4Mo. The dotted line outlines the portion traced, and the notations for Ni_2Mo and Ni_4Mo positions are the same as in Fig. 1.

Fig. 4. $[\bar{1}30]$ electron diffraction pattern of quenched Ni_4Mo.

Fig. 5. (a) [110] diffraction pattern of Ni_4Mo. (b) the indexed pattern.

Fig. 6. Diffraction patterns of Ni_3Mo after quenching in iced brine from 1270°C (a) [001] pattern (b) [110] pattern.

Fig. 7. Ni_3Mo samples after aging for 1 hour at 650°C (a) Dark field micrograph of $\{1\frac{1}{2}0\}$ spot encircled in the diffraction pattern; (b) the $[1\bar{2}0]$ diffraction pattern corresponding to (a).

Fig. 8. Evaporated thin film of Au_3Cr after aging for 67 hrs at 270°C (a) [001] orientation, (b) $[\bar{1}30]$ orientation.

Fig. 9. (a) [001] diffraction pattern of Au_3Cr film taken at 330° ± 10°C; (b) $[\bar{1}30]$ pattern of same Au_3Cr film taken at 370°C.

Fig. 10. Electron diffraction patterns of bulk Au_3Cr after quenching in water from 550°C. (a) [001] pattern, (b) $[\bar{1}30]$ pattern.

Fig. 11. (a) [121] diffraction pattern of bulk Au_3Cr, quenched into water (b) the indexed pattern.

Fig. 12. Three-dimensional reciprocal lattice models of Au_3Cr showing (a) the distribution of diffuse scattering in the sro state, (b) the six variants of Dla in the ℓro state.

Fig. 13. [001] diffraction pattern of bulk Au_4V quenched in iced brine from 900°C.

Fig. 14. (a) [001] diffraction pattern of evaporated thin film of Au_3Mn showing two-dimensional long period superstructure (Watanabe type), (b) another [001] pattern showing additional Dla superlattice spots, (c) sketch of [001] pattern corresponding to Watanabe type structure.

Fig. 15. (a) [001] diffraction pattern of ordered thin film of Au_3Mn taken at 450°C, (b) the same pattern as (a) but taken at 500°C.

Fig. 16. Theoretical diffuse scattering map for Ni_3Mo.

Fig. 17. Theoretical diffuse scattering map for Au_3Mn.

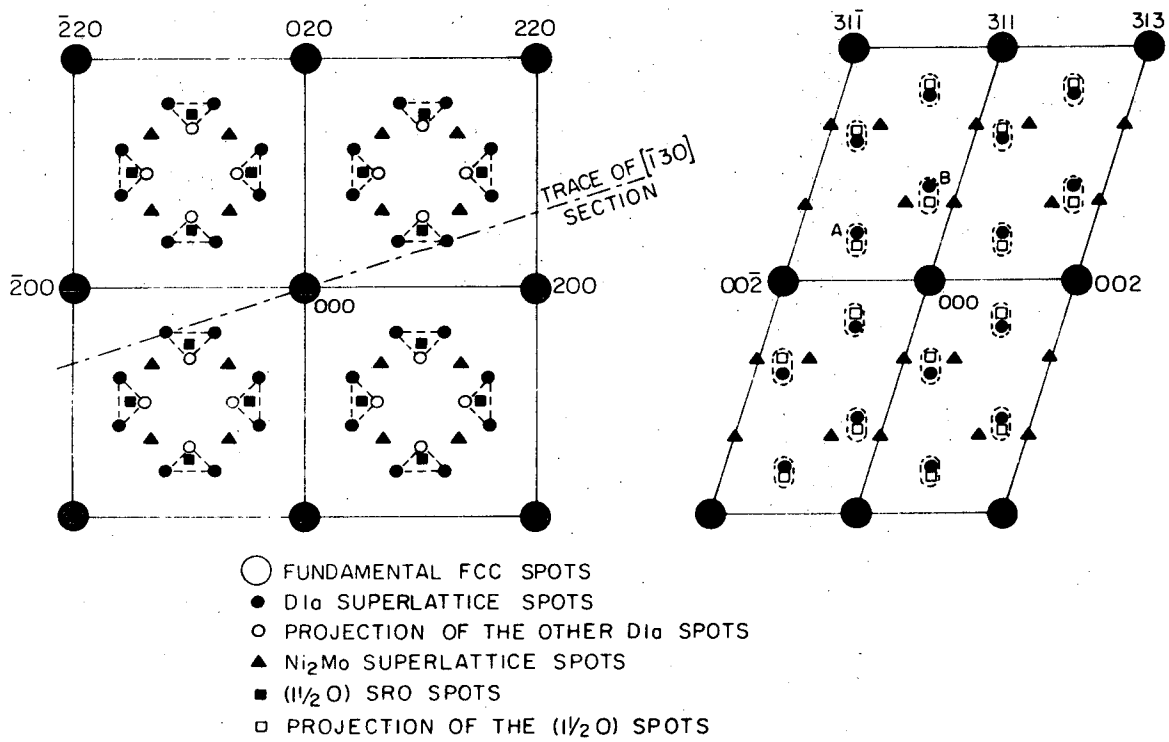

XBL717-7009

Fig. 1

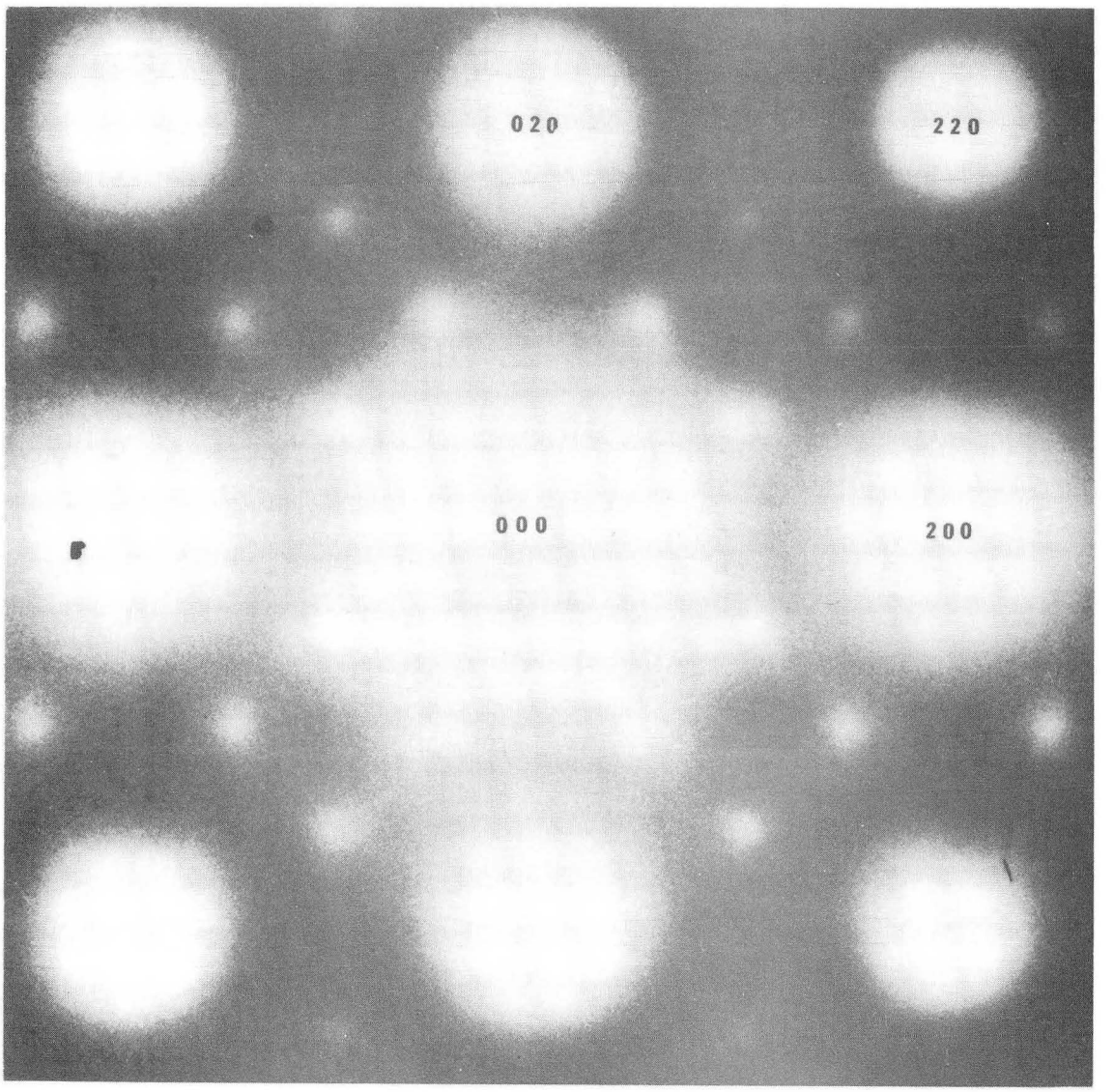

XBB 717-3401A

Fig. 2

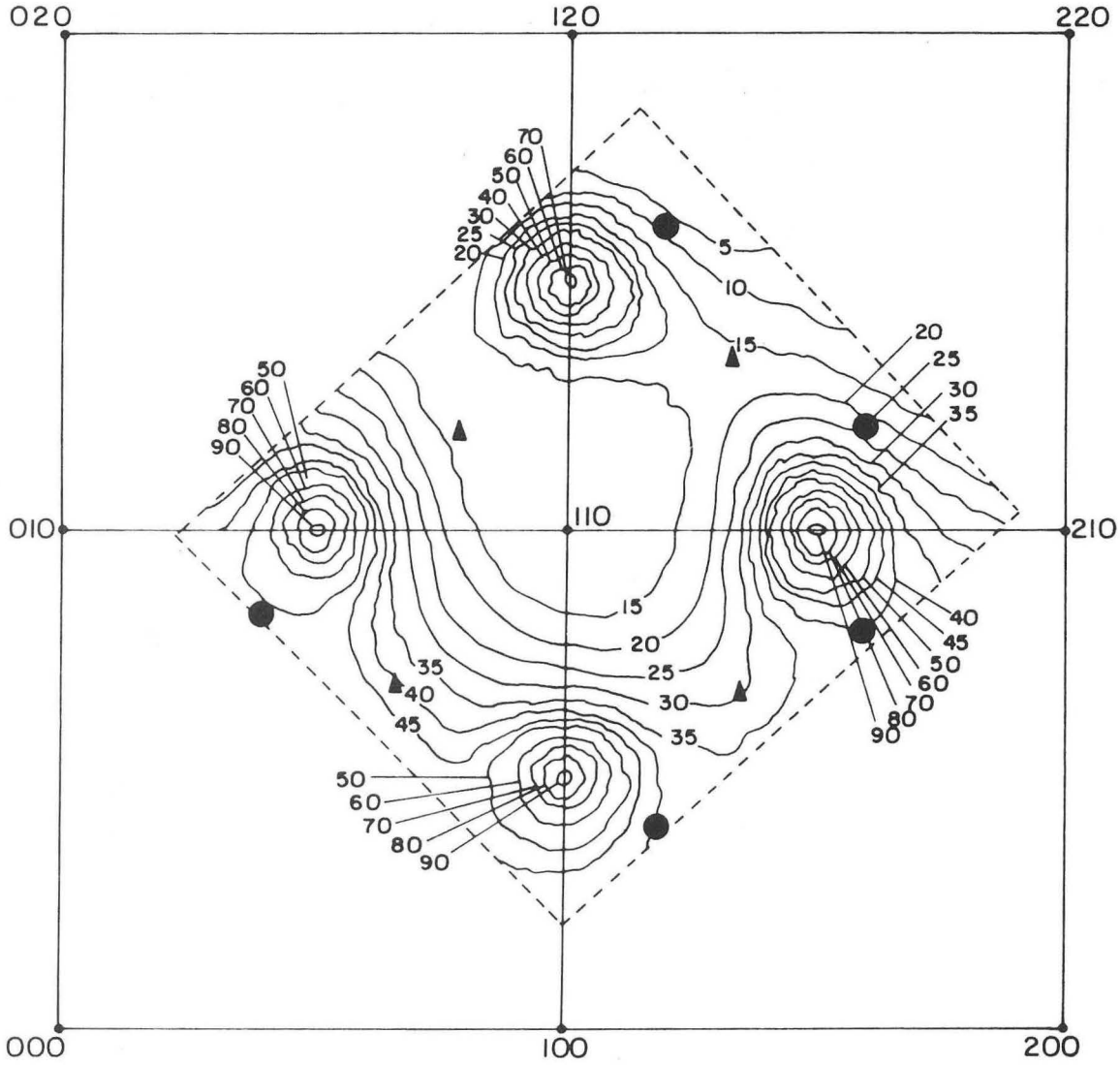

XBL7110-7338

Fig. 3

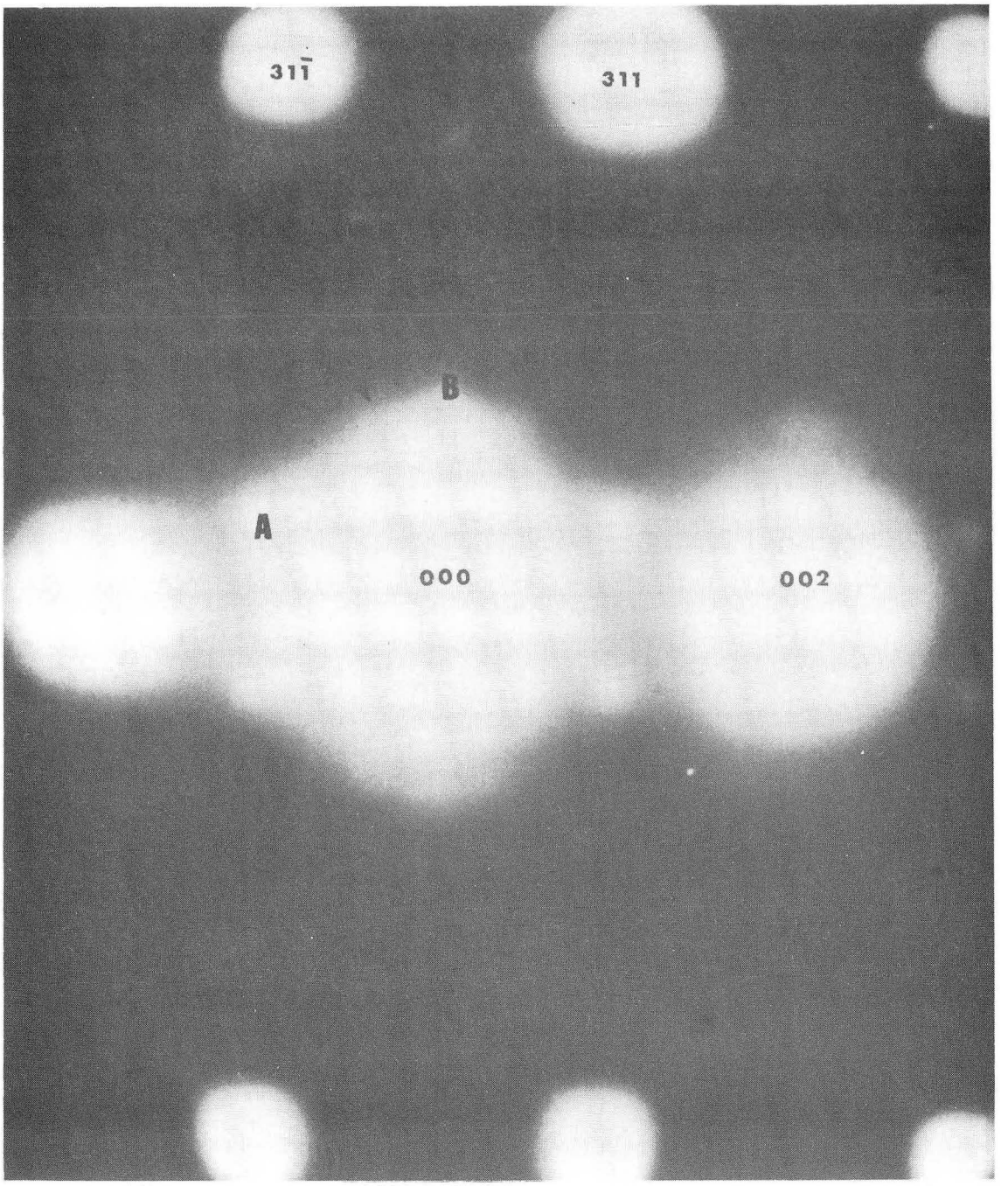

XBB 717-3407A

Fig. 4

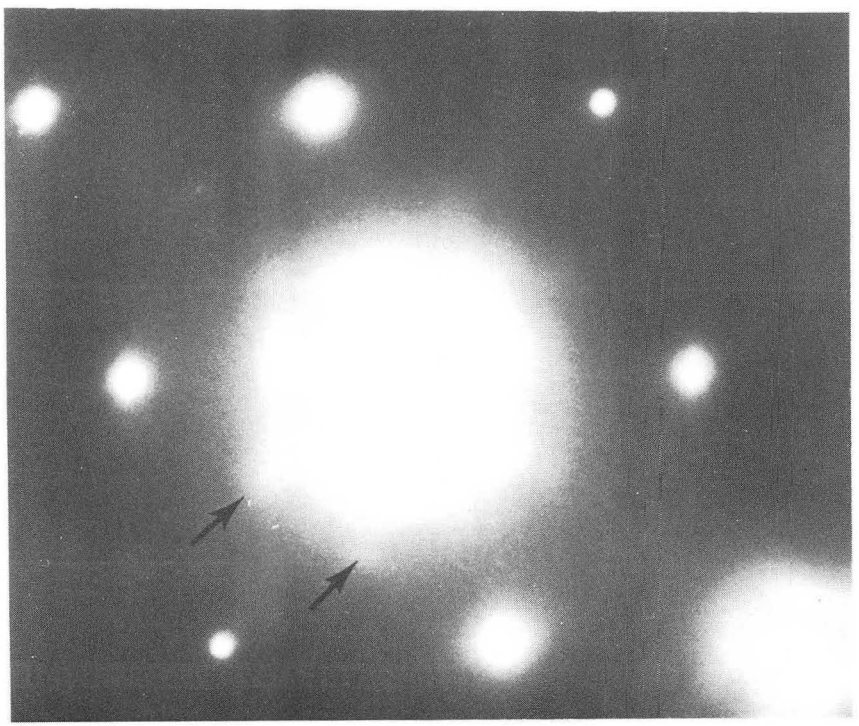

A

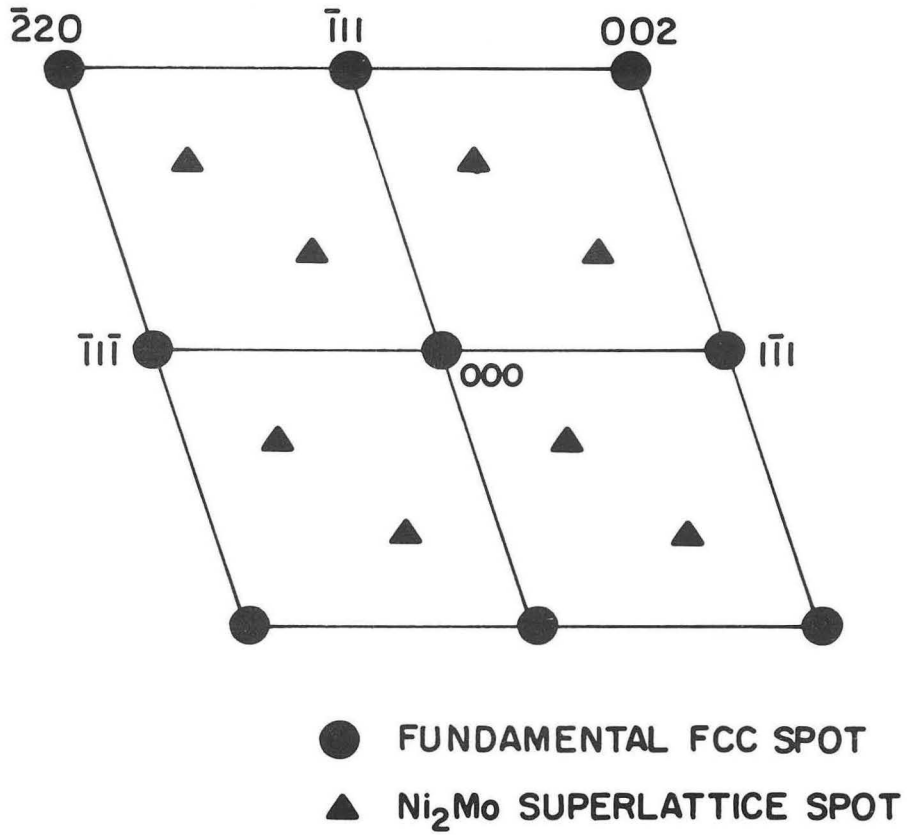

B

XBB 717-3397

Fig. 5

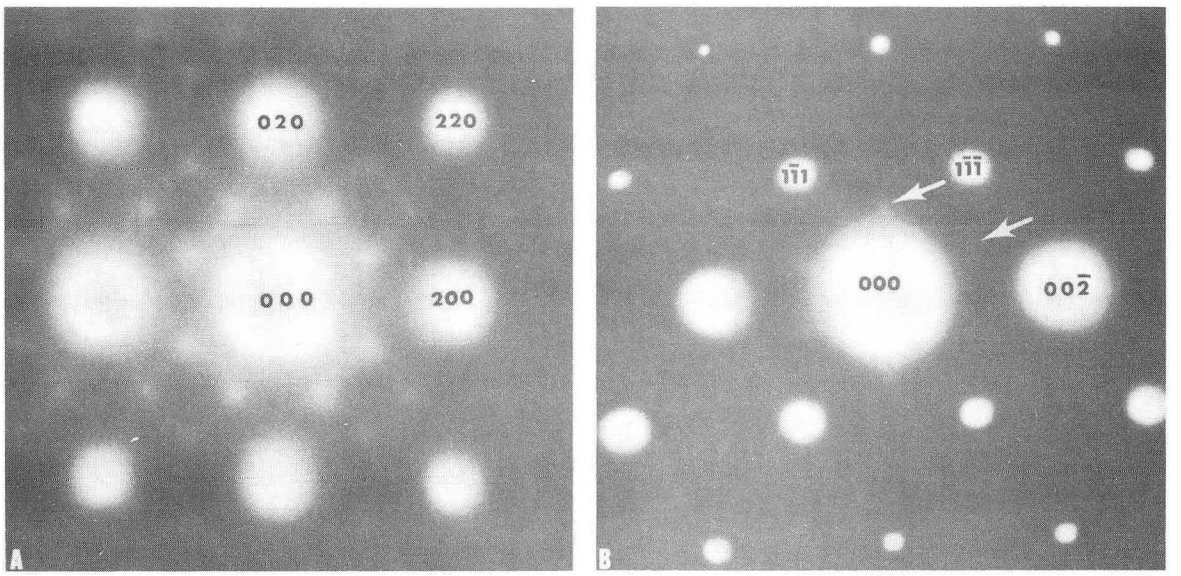

XBB 717-3406A

Fig. 6

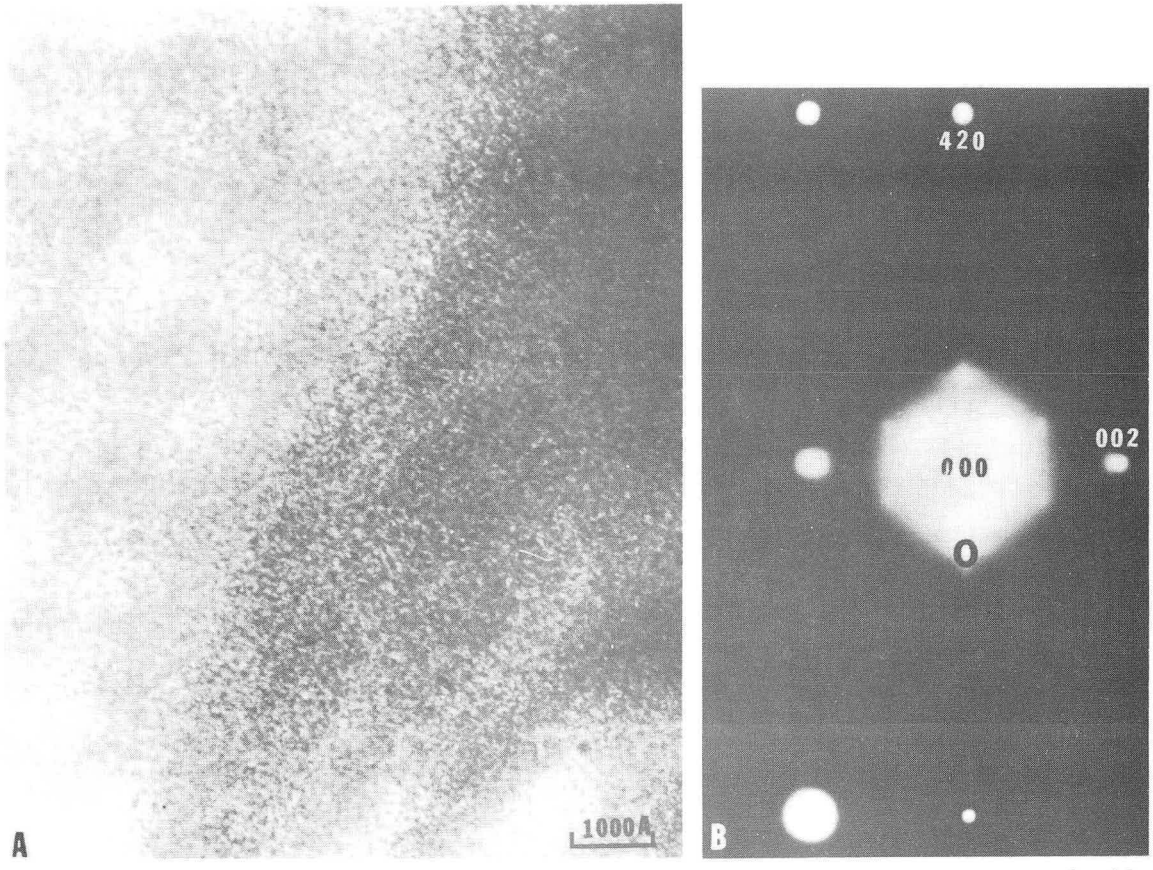

XBB 7110-4766A

Fig. 7

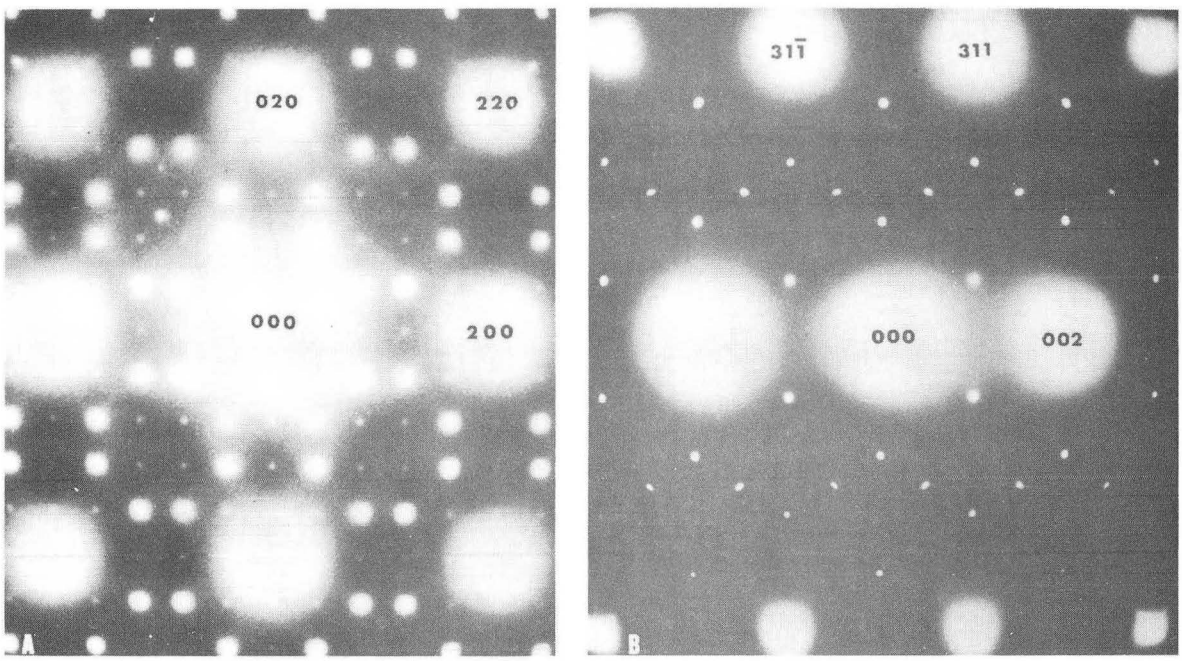

XBB 717-3405A

Fig. 8

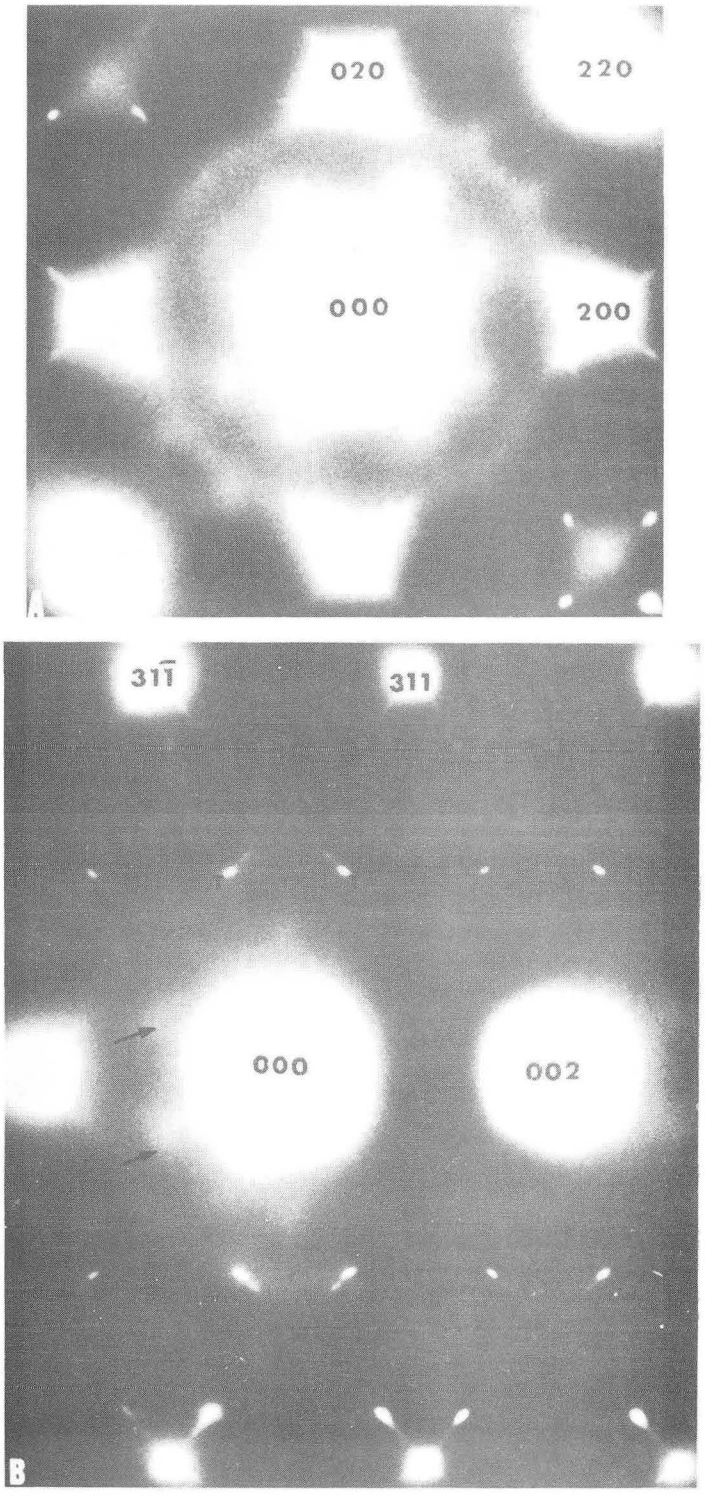

XBB 717-3401A

Fig. 9

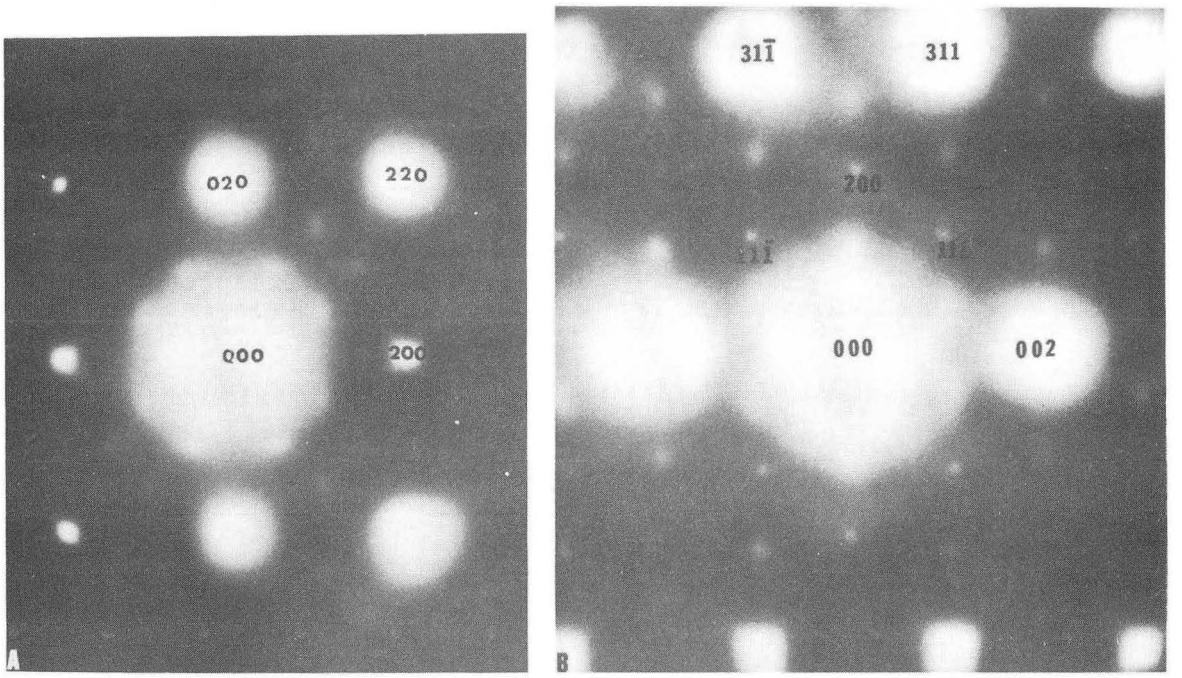

XBB 717-3404A

Fig. 10

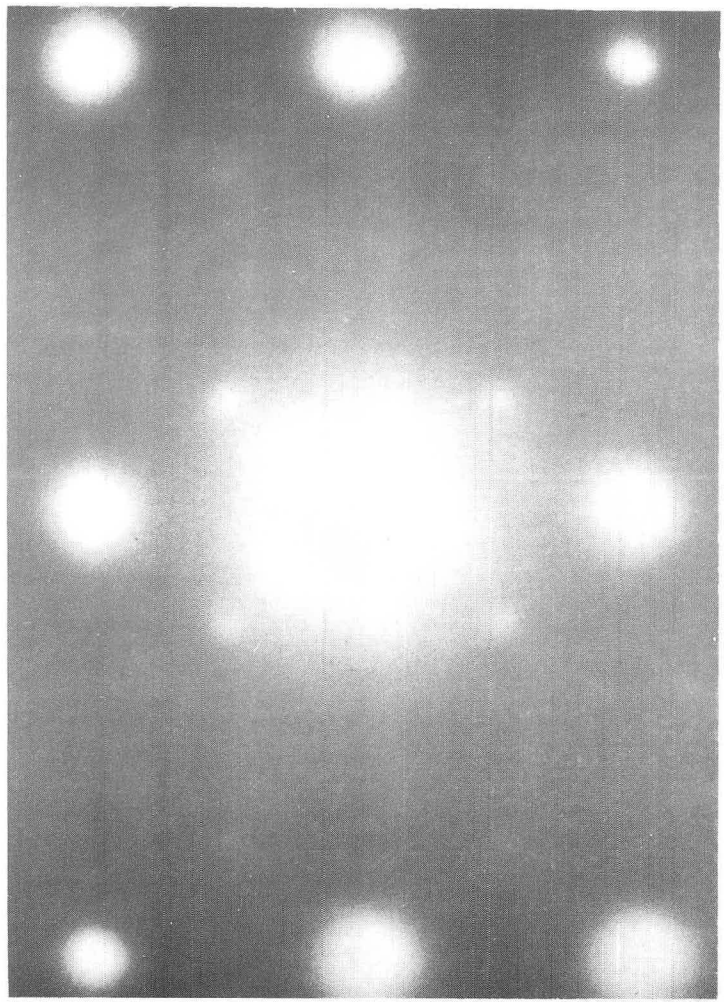

A

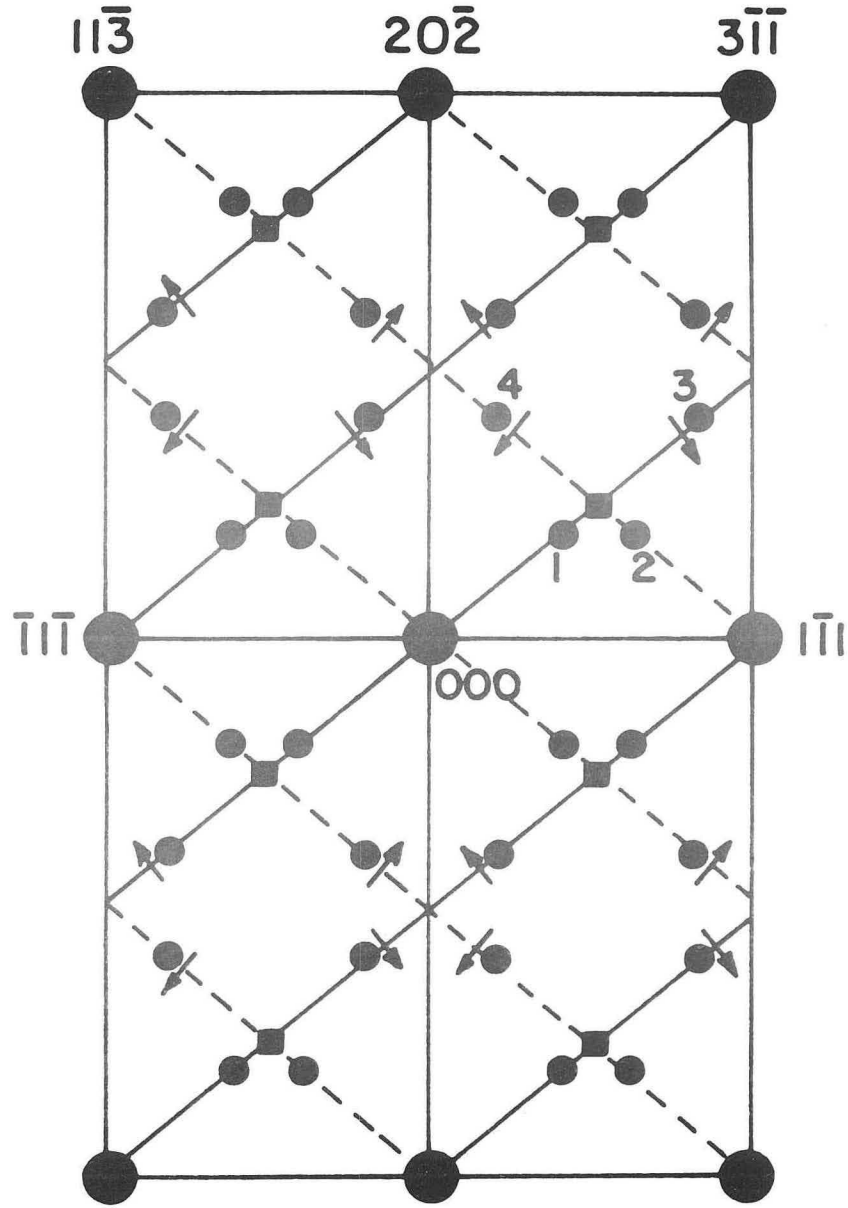

B

XBB 717-3396

Fig. 11

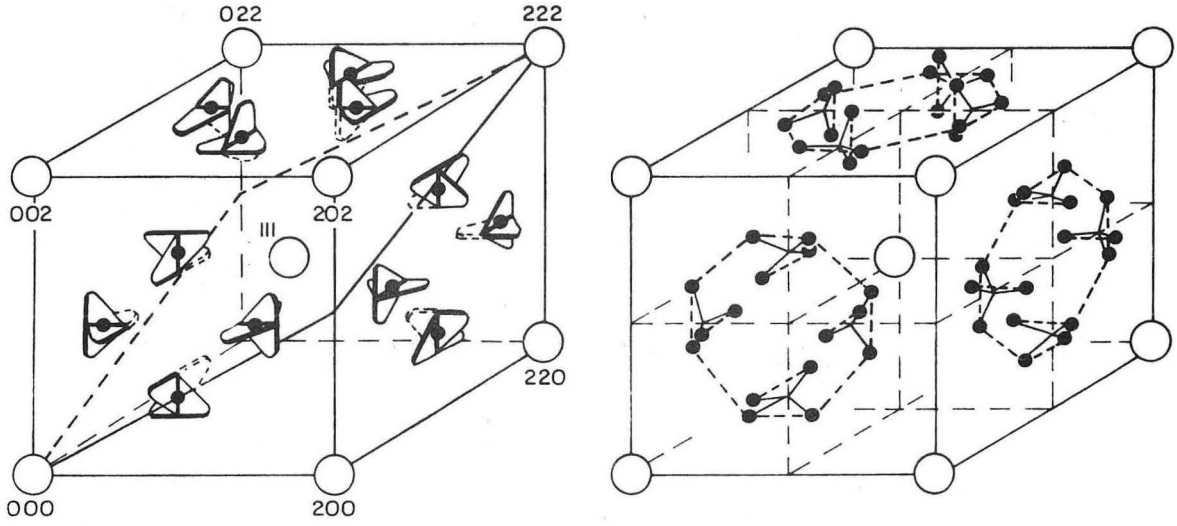

Disordered state

LRO state: 6 variants of D1a

Reciprocal lattices of Au_3Cr

XBL713-6626

Fig. 12

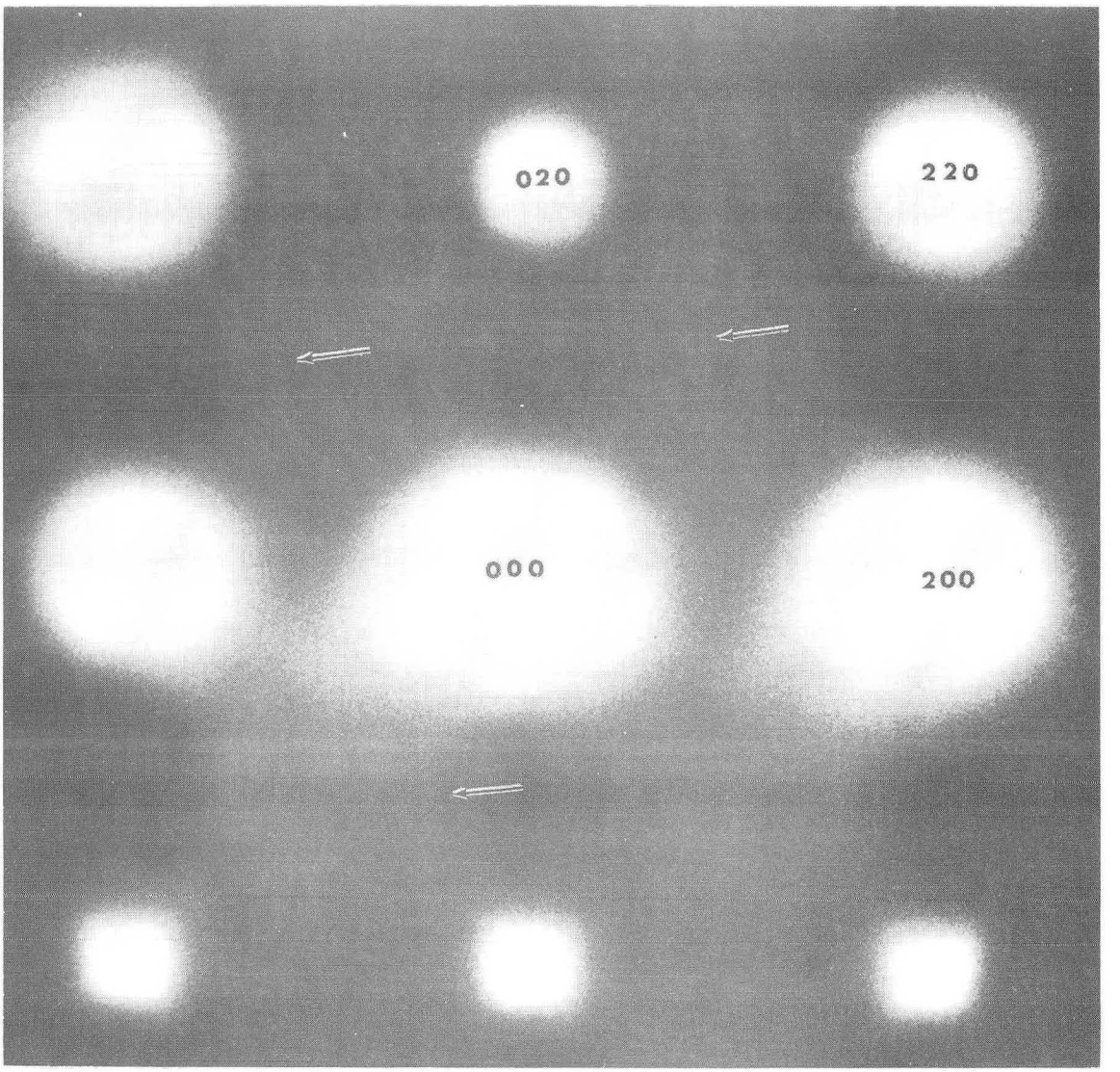

XBB 717-3399A

Fig. 13

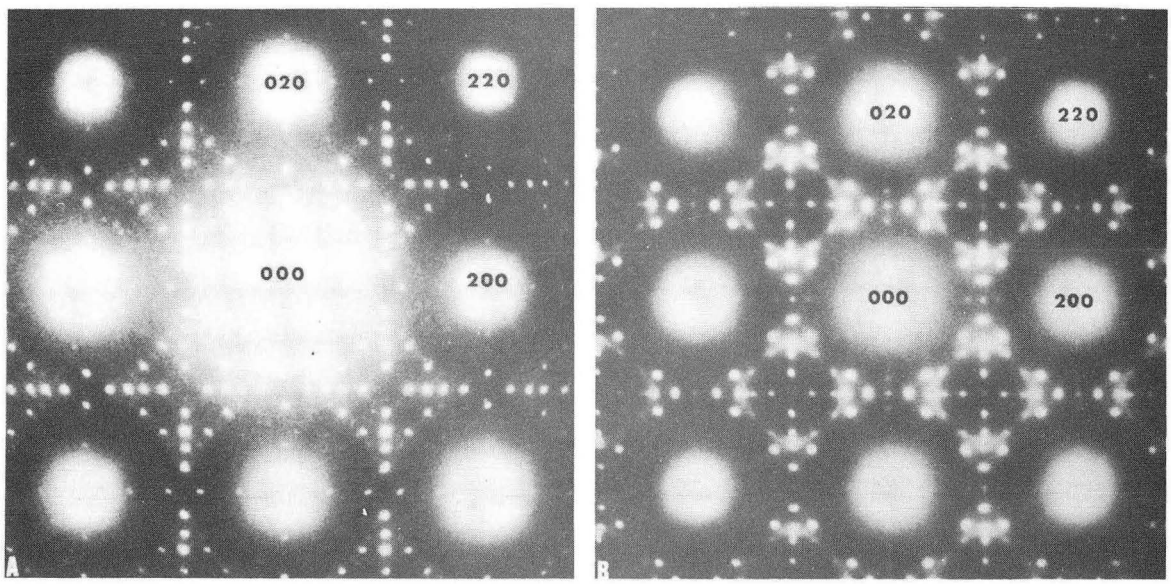

XBB 717-3414A

Fig. 14

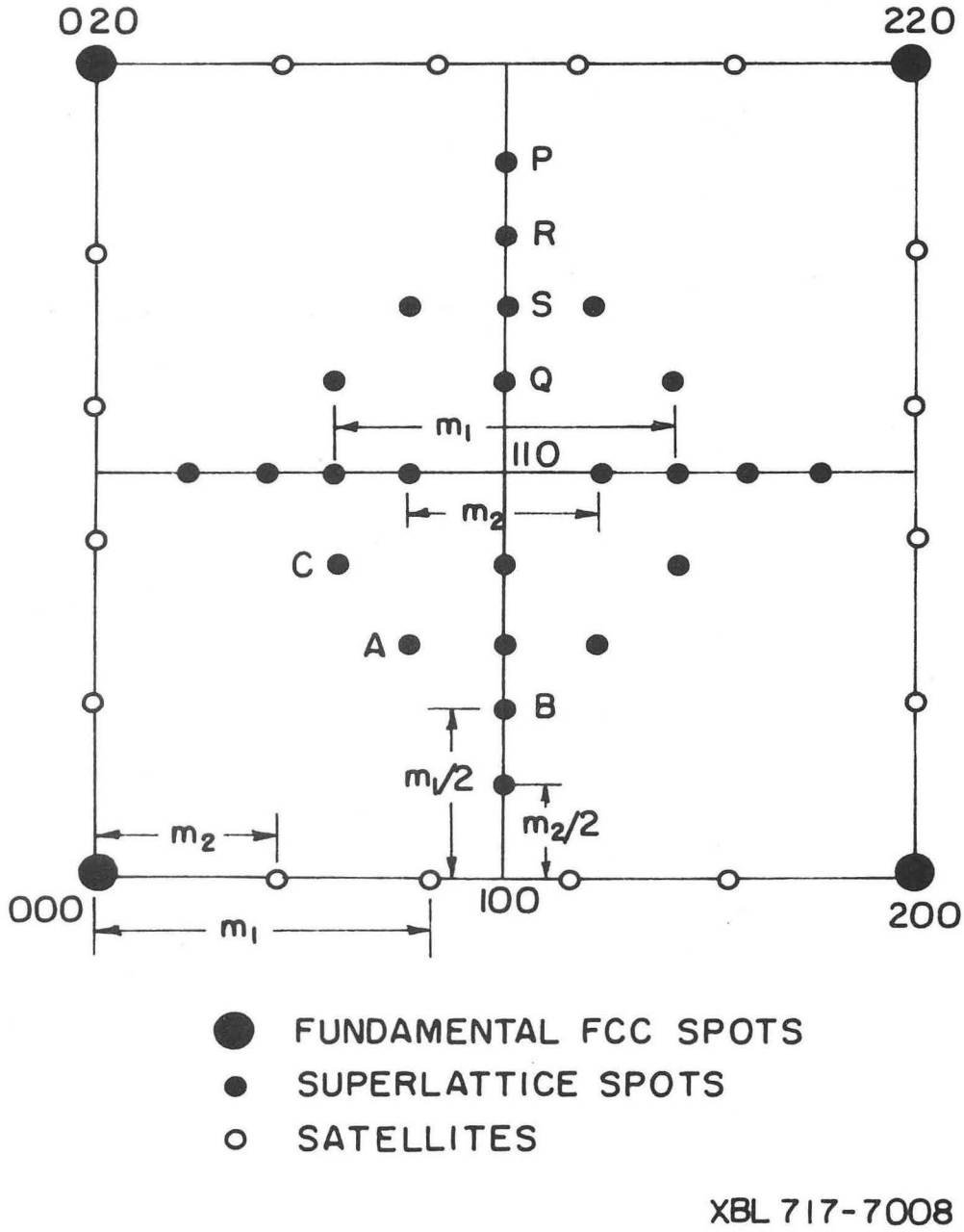
020
220
P
R
S
Q
m1
110
m2
C
A
B
m1/2
m2/2
m2
000
100
200
m1
FUNDAMENTAL FCC SPOTS
SUPERLATTICE SPOTS
SATELLITES
XBL 717-7008

Fig. 14 (cont.)

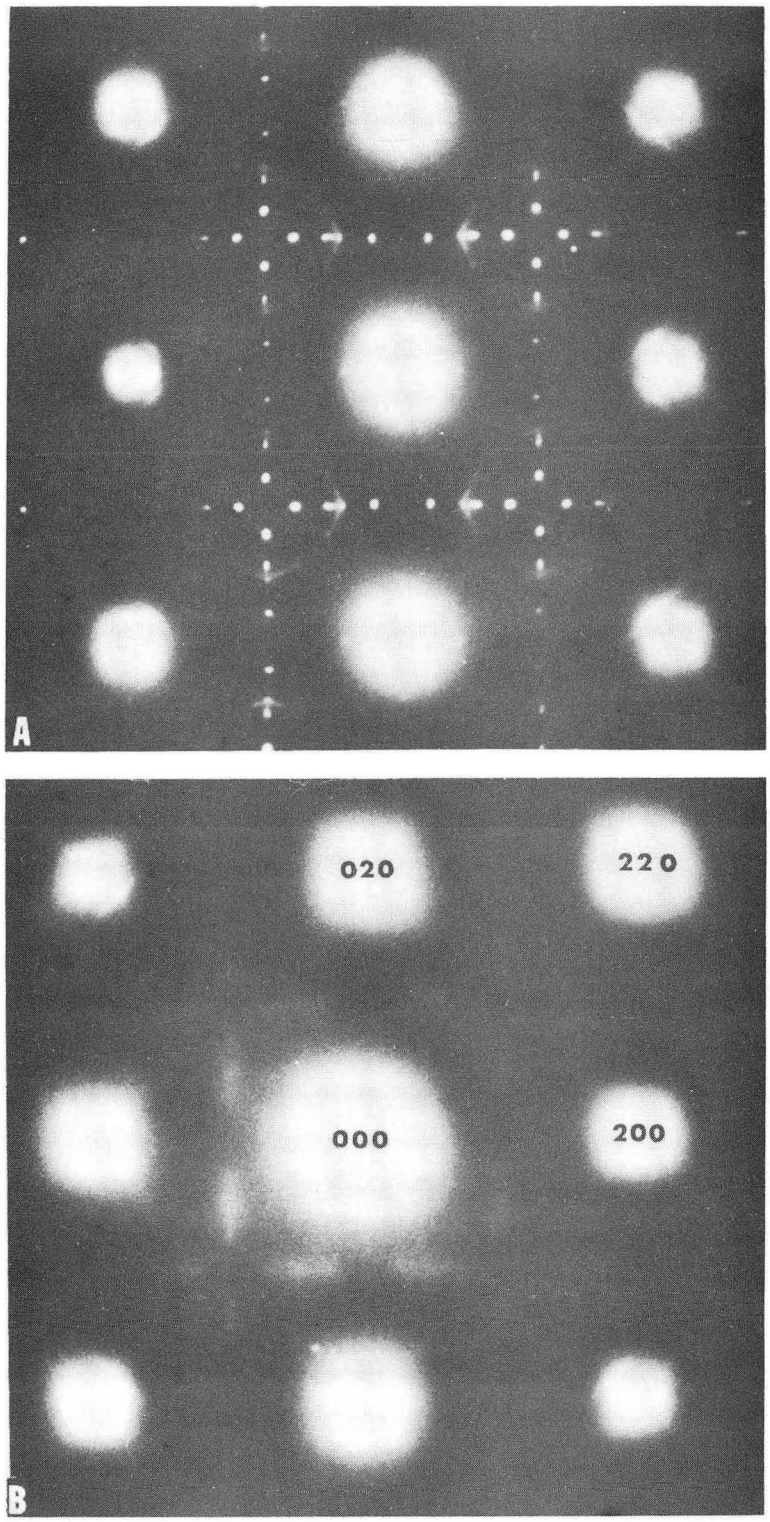

XBB 7110-4762A

Fig. 15

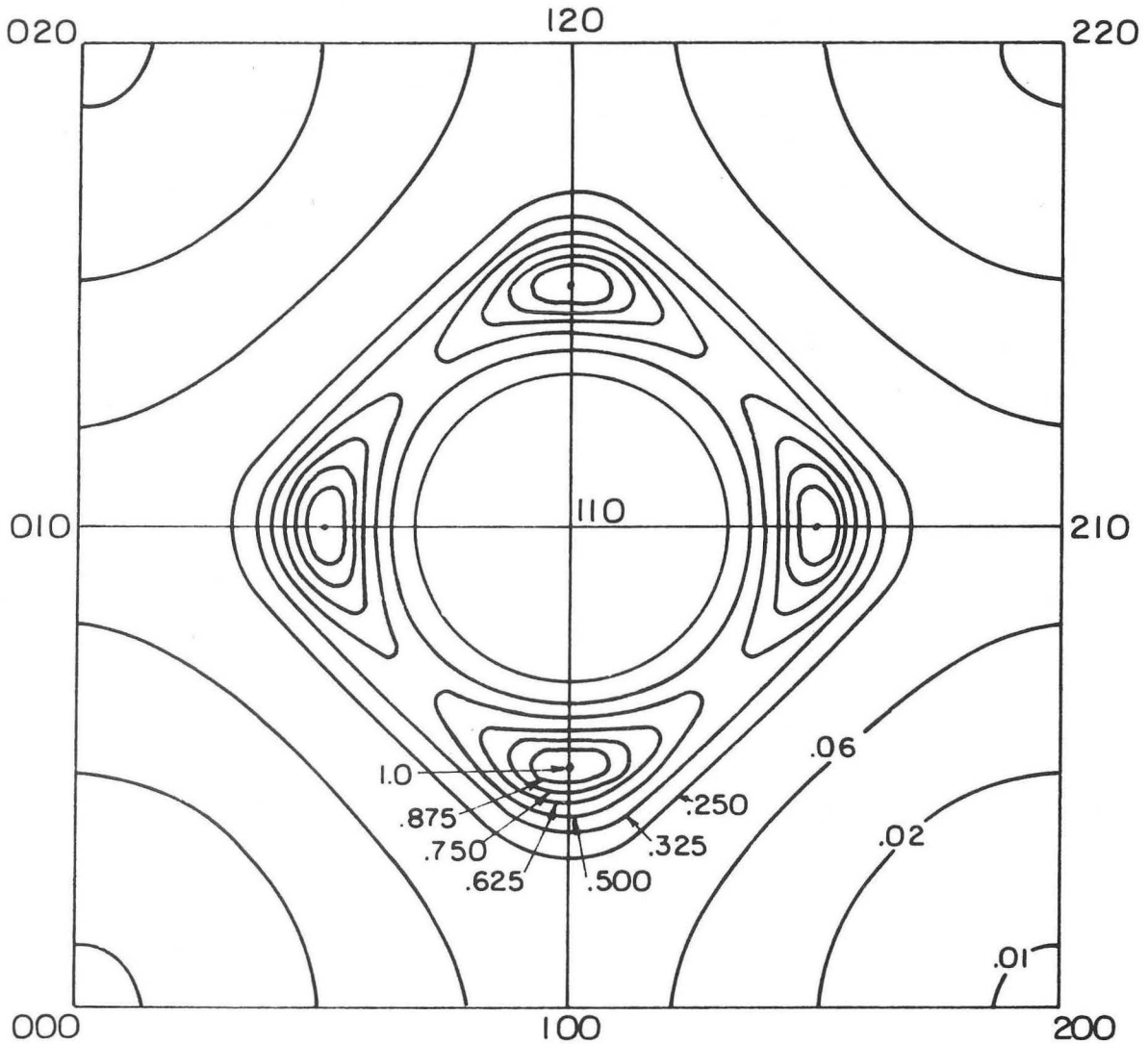

$T_c/T = 0.95$; $V_2/V_1 = 0.4$; $V_3/V_1 = 0.00$

XBL 717- 7007

Fig. 16

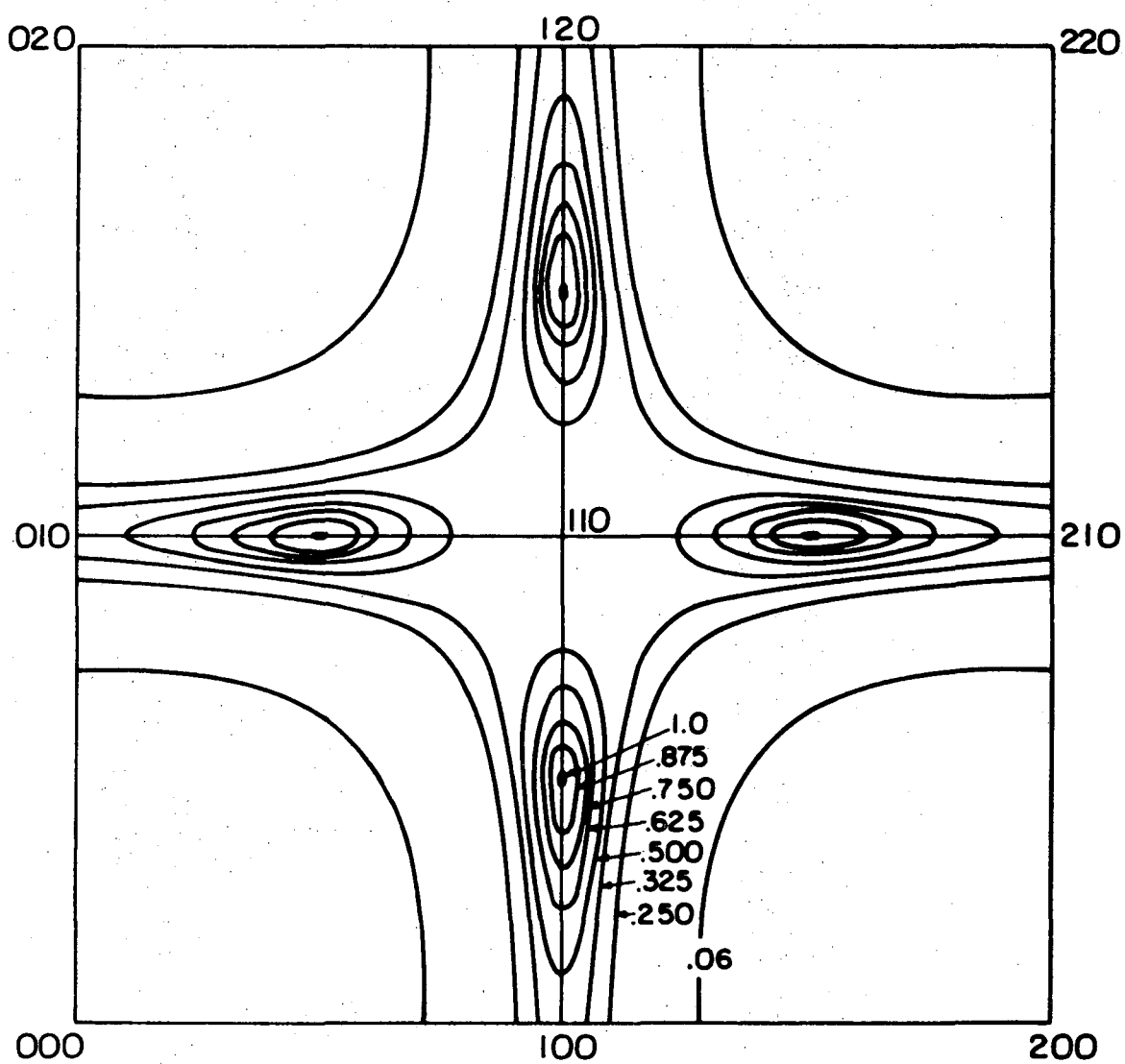

$T_c/T = 0.95$; $V_2/V_1 = -0.7$; $V_3/V_1 = -0.2$

XBL717-7010

Fig. 17

LEGAL NOTICE

This report was prepared as an account of Government sponsored work. Neither the United States, nor the Commission, nor any person acting on behalf of the Commission:

A. Makes any warranty or representation, expressed or implied, with respect to the accuracy, completeness, or usefulness of the information contained in this report, or that the use of any information, apparatus, method, or process disclosed in this report may not infringe privately owned rights; or

B. Assumes any liabilities with respect to the use of, or for damages resulting from the use of any information, apparatus, method, or process disclosed in this report.

As used in the above, "person acting on behalf of the Commission" includes any employee or contractor of the Commission, or employee of such contractor, to the extent that such employee or contractor of the Commission, or employee of such contractor prepares, disseminates, or provides access to, any information pursuant to his employment or contract with the Commission, or his employment with such contractor.

TECHNICAL INFORMATION DIVISION
LAWRENCE RADIATION LABORATORY
UNIVERSITY OF CALIFORNIA
BERKELEY, CALIFORNIA 94720